A thermal stress finite element analysis of beam structures by hierarchical modelling

A thermal stress finite element analysis of beam structures by hierarchical modelling

G. Giunta[*],
Luxembourg Institute of Science and Technology,
5, avenue des Hauts-Fourneaux, L-4362 Esch-sur-Alzette, Luxembourg

G. De Pietro[†],
Luxembourg Institute of Science and Technology,
5, avenue des Hauts-Fourneaux, L-4362 Esch-sur-Alzette, Luxembourg and
Politecnico di Torino, c.so Duca degli Abruzzi 24, 10129 Turin, Italy

H. Nasser[‡], S. Belouettar[§],
Luxembourg Institute of Science and Technology,
5, avenue des Hauts-Fourneaux, L-4362 Esch-sur-Alzette, Luxembourg

E. Carrera[¶], M. Petrolo[‖],
Politecnico di Torino,
c.so Duca degli Abruzzi 24, 10129 Turin, Italy

Author for correspondence:
Gabriele De Pietro, Ph.D. student,
Materials Research and Technology Department,
Luxembourg Institute of Science and Technology,
5, avenue des Hauts-Fourneaux,
L-4362 Esch-sur-Alzette, Luxembourg.
tel: +352 275 888 1,
fax: +352 275 885,
e-mail: gabriele.depietro@list.lu

[*]Research scientist.
[†]Ph.D. student.
[‡]Research scientist.
[§]Research Scientist.
[¶]Full Professor.
[‖]Research scientist.

Abstract

In this study, the thermoelastic behaviour of three-dimensional isotropic and laminated beams is investigated. The three-dimensional beam is modelled through advanced one-dimensional finite elements derived via hierarchical expansion of the displacements over the cross-section. The approximation order of the displacement field is a free parameter that leads to the formulation of a family of several beam elements. The number of nodes per element is also a free parameter. Linear, quadratic and cubic variations along the beam axis are considered within the element. The temperature field is treated as an external load within the mechanical analysis and it is obtained by exactly solving Fourier's heat conduction equation. The governing algebraic equations are obtained via the Principle of Virtual Displacements. Displacements and stresses are investigated and results are validated towards three-dimensional FEM solutions. The temperature load results in a three-dimensional stress state that calls for accurate models. Numerical investigations show that the proposed finite elements yield accurate yet computationally efficient results.

Keywords: Beam structures, Hierarchical modelling, One-dimensional finite elements, Thermo-mechanical response, Composite materials.

1 Introduction

Isotropic and laminated one-dimensional structural components subjected to thermal solicitations can be commonly found in applications in several fields such as aeronautics, space, automotive and civil engineering. The thermo-mechanical behaviour of beam-like structures is clearly three-dimensional and an accurate prediction calls for refined higher-order models. Many different approaches have been used over the last years and a brief overview is here presented.

A general overview on thermal stresses analysis can be found in Boley and Weiner [1] and Hetnarski and Eslami [2]. The study of the vibrations of a cantilever damped Timoshenko beam in presence of thermal gradients has been carried out by Gu et al. [3]. Conservation of energy was used to obtain the motion equations and, finally, an analytical solution of the coupling problem was provided. Constant temperature at the clamped end and adiabatic conditions at the free-end were considered. On the top surface and bottom surface of the beam, boundary conditions were given according to the convection coefficients. No heat conduction was considered along the width and Fourier's heat conduction equation was solved by separation of variables. Pakade et al. [4] provided an exact analytical solution for displacements and stresses for a rectangular isotropic beam under thermal stresses. The temperature field was obtained by solving Fourier's heat conduction equation with generic temperature boundary conditions by means of Marchi-Fasulo's transform over the cross-section coordinates and Fourier sine transform along the axis. Sadowski et al. [5] studied the thermo-mechanical behaviour of a layered thin-walled cylinder beam. One-dimensional Cosserat mechanical model for multi-layered beams with constant displacements over the cross-section was used in order to predict the displacement field. A linear temperature distribution along the axis and constant distribution over the cross-section were considered. Lezgy-Nazargah [6] studied bi-directional FGM beams under thermal stresses. The displacement field was assumed as the combination of polynomials and exponential functions. The temperature field was approximated by a Hermite interpolation along the thickness direction. As far as the axial variation is concerned, non-uniform rational basis-spline functions were used. The governing equations were obtained from the principle of stationary potential energy. Jeon et al. [7] performed a multi-scale analysis of a fibre-reinforced polymer composite sandwich beam under thermal and mechanical loads using solid finite elements. Two-dimensional thermoelastic analyses of variable thickness isotropic beams were carried out by Xu and Zhou [8]. The displacement field was considered as a sinus expansion along the axis and the unknown displacement profile along the thickness was obtained by solving the differential equilibrium equations. The temperature profile was obtained by analytically solving the heat conduction equation. Carpinteri and Paggi [9] carried out a thermo-elastic analytical stress analysis of multi-layered beams by means of Euler-Bernoulli's kinematic hypotheses. A conforming three-node thermo-mechanical beam finite element based upon a sinus-refined kinematic model was derived by Vidal and Polit [10] for the analysis of laminated beams. Kapuria et al. [11] studied the thermal stresses in laminated simply supported beams by a higher-order zig-zag theory. A piecewise linear function along the through-the-thickness direction was used for the temperature. The principle of virtual work was used to derive the governing equations and Navier-type solution was used. Ghiringhelli [12] presented a finite element semi-discretisation for composite beams in which the temperature distribution within the beam cross-section was computed by a two-dimensional finite element analysis. Comparisons with three-dimensional finite element analysis were presented. In this paper, a

thermoelastic analysis of isotropic and laminated orthotropic beams is carried out via refined one-dimensional finite elements. A family of higher-order beam elements is formulated by a compact form of the a priori displacement field approximation over the cross-section. The kinematic description over the cross-section can be, therefore, freely enriched by varying the approximation order. Cross-section in- and out-of-plane warping is, then, straightforwardly and implicitly accounted for. This Unified Formulation (UF) also allows deriving finite elements with a generic number of nodes. Linear, quadratic and cubic C^0 elements are used in the numerical investigations. UF had been previously proposed for plate and shell structures, see Carrera [13] and it has been lately extended to beams, see Carrera et al. [14], Carrera and Giunta [15], Giunta et al. [16, 17, 18], Catapano et al. [19] and Polit et al. [20]. Stemming from UF, He et al. [21] proposed a multi-scale method for the mechanical modelling of sandwich structures, whereas a wrinkling analysis of stiff thin films resting on a thick elastic substrate was carried out by Yang et al. [22]. As far as thermal stress analyses of beams are concerned, UF has been used in the framework of strong form approaches such as Navier-type [23] and point collocation [24] solutions. The novelty of the present work consists in the use of the finite element method to solve, in a weak sense, the governing differential equations governing the problem. Shear locking is avoided by a classical selective integration procedure, see Bathe [25] that is effective regardless the approximation order over the cross-section. These latter are obtained through the principle of virtual displacements in the form of a fundamental nucleus that is unique regardless the order of expansion of the displacement field as well as the number of nodes per element. A classical one-way staggered solution method is used (see Nowiski [26]): the temperature field is first obtained by solving the Fourier heat conduction equation by a Navier-type closed form solution and a mechanical analysis is, then, carried out accounting for the temperature as an external loading. Results are provided in terms of displacements and stresses. They are validated through comparison with three-dimensional finite element solutions showing that the thermo-elastic response of beams, which is actually three-dimensional, can be accurately described with reduced computational costs.

2 Displacement Field Approximation

A Cartesian reference system is adopted, see Fig. 1: the x coordinate is aligned with the direction of the longitudinal axis of the beam; y- and z-axis are two orthogonal directions laying on the plane of the cross-section Ω. The displacement vector is:

$$\mathbf{u}^T(x,y,z) = \left\{ \begin{array}{ccc} u_x(x,y,z) & u_y(x,y,z) & u_z(x,y,z) \end{array} \right\} \tag{1}$$

where u_x, u_y and u_z are the components along x-, y- and z-axis and superscript "T" represents the transposition operator.

The displacement field is a priori assumed over the cross-section in the following manner:

$$\mathbf{u}(x,y,z) = F_\tau(y,z)\,\mathbf{u}_\tau(x) \quad \text{with} \quad \tau = 1,\ 2,\ \ldots,\ N_u \tag{2}$$

According to the Einstein's notation, subscript τ implicitly represents a summation. $F_\tau(y,z)$ is a generic expansion function over the cross-section and N_u is the number of accounted terms.

This kinematic formulation allows to account for several beam theories since the choice of the expansion functions $F_\tau(y,z)$ and N_u is arbitrary. In this study, Mac Laurin's polynomials are used as approximating functions F_τ. N_u and F_τ as functions of the order of the theory N are obtained through Pascal's triangle as

shown in Table 1.

The explicit form of a generic N-order displacement field reads:

$$\begin{aligned} u_x &= u_{x1} + u_{x2}y + u_{x3}z + \cdots + u_{x\frac{(N^2+N+2)}{2}}y^N + \cdots + u_{x\frac{(N+1)(N+2)}{2}}z^N, \\ u_y &= u_{y1} + u_{y2}y + u_{y3}z + \cdots + u_{y\frac{(N^2+N+2)}{2}}y^N + \cdots + u_{y\frac{(N+1)(N+2)}{2}}z^N, \\ u_z &= u_{z1} + u_{z2}y + u_{z3}z + \cdots + u_{z\frac{(N^2+N+2)}{2}}y^N + \cdots + u_{z\frac{(N+1)(N+2)}{2}}z^N. \end{aligned} \tag{3}$$

As far as the displacements variation along the beam axis is concerned, a one-dimensional finite element approximation is used:

$$\mathbf{u}\left(x,y,z\right) = F_\tau\left(y,z\right) N_i\left(x\right) \mathbf{q_{\tau i}} \;\text{ with }\; \tau = 1,\ 2,\ \ldots,\ N_u \;\text{ and }\; i = 1,\ 2,\ \ldots,\ N_n^e \tag{4}$$

$N_i\left(x\right)$ is a C^0 shape function, N_n^e the number of nodes per element and $\mathbf{q_{\tau i}}$ the nodal displacement unknown vector. Linear, quadratic and cubic elements based on Lagrangian shape functions are considered. They are referred to as "B2", "B3" and "B4", respectively.

3 Gemetrical and Constitutive Equations

The total strain vector, $\boldsymbol{\varepsilon}_t$, is grouped into a vector $\boldsymbol{\varepsilon}_{tn}$ with components in the longitudinal direction and a vector $\boldsymbol{\varepsilon}_{tp}$ with components laying on the cross-section planes:

$$\boldsymbol{\varepsilon}_{tn}^T = \left\{ \begin{array}{ccc} \varepsilon_{txx} & \varepsilon_{txy} & \varepsilon_{txz} \end{array} \right\}, \quad \boldsymbol{\varepsilon}_{tp}^T = \left\{ \begin{array}{ccc} \varepsilon_{tyy} & \varepsilon_{tzz} & \varepsilon_{tyz} \end{array} \right\}. \tag{5}$$

Under the hypothesis of geometrical linearity, the strain-displacement relation is given by:

$$\begin{aligned} \boldsymbol{\varepsilon}_{tn}^T &= \left\{ \begin{array}{ccc} u_{x,_x} & u_{x,_y} + u_{y,_x} & u_{x,_z} + u_{z,_x} \end{array} \right\}, \\ \boldsymbol{\varepsilon}_{tp}^T &= \left\{ \begin{array}{ccc} u_{y,_y} & u_{z,_z} & u_{y,_z} + u_{z,_y} \end{array} \right\}. \end{aligned} \tag{6}$$

Subscripts "x", "y" and "z" preceded by comma mean derivation versus the corresponding coordinate.

Eqs. (6) can be written in a matrix form as follows:

$$\begin{aligned} \boldsymbol{\varepsilon}_{tn} &= \mathbf{D}_{np}\mathbf{u} + \mathbf{D}_{nx}\mathbf{u}, \\ \boldsymbol{\varepsilon}_{tp} &= \mathbf{D}_{p}\mathbf{u}. \end{aligned} \tag{7}$$

$\mathbf{D}_{np}$, $\mathbf{D}_{nx}$, and $\mathbf{D}_p$ are the following differential matrix operators:

$$\mathbf{D}_{np} = \begin{bmatrix} 0 & 0 & 0 \\ \dfrac{\partial}{\partial y} & 0 & 0 \\ \dfrac{\partial}{\partial z} & 0 & 0 \end{bmatrix}, \quad \mathbf{D}_{nx} = \mathbf{I}\frac{\partial}{\partial x}, \quad \mathbf{D}_p = \begin{bmatrix} 0 & \dfrac{\partial}{\partial y} & 0 \\ 0 & 0 & \dfrac{\partial}{\partial z} \\ 0 & \dfrac{\partial}{\partial z} & \dfrac{\partial}{\partial y} \end{bmatrix} \tag{8}$$

and $\mathbf{I}$ the unit matrix.

According to the displacement field in Eq.(4), Eqs. (7) in terms of the nodal unknowns become:

$$\begin{aligned} \boldsymbol{\varepsilon}_{tn} &= \mathbf{D}_{np}F_\tau N_i \mathbf{q_{\tau i}} + \mathbf{D}_{nx}F_\tau N_i \mathbf{q_{\tau i}}, \\ \boldsymbol{\varepsilon}_{tp} &= \mathbf{D}_{p}F_\tau N_i \mathbf{q_{\tau i}}. \end{aligned} \tag{9}$$

The stress vector is also arranged according to their axial and in-plane components:

$$\boldsymbol{\sigma}_p^T = \left\{ \begin{array}{ccc} \sigma_{yy} & \sigma_{zz} & \sigma_{yz} \end{array} \right\}, \quad \boldsymbol{\sigma}_n^T = \left\{ \begin{array}{ccc} \sigma_{xx} & \sigma_{xy} & \sigma_{xz} \end{array} \right\}. \tag{10}$$

In the case of a thermo-elastic analysis, Hooke's law reads:

$$\boldsymbol{\sigma} = \mathbf{C}^k \boldsymbol{\varepsilon}_e = \mathbf{C}^k \left(\boldsymbol{\varepsilon}_t - \boldsymbol{\alpha}^k T \right) = \mathbf{C}^k \boldsymbol{\varepsilon}_t - \boldsymbol{\lambda}^k T, \tag{11}$$

where subscript "e" stands for elastic deformation and superscript "k" refers to the k-th layer of a multi-layered beam. $\mathbf{C}^k$ is the material elastic stiffness matrix in a generic reference system, $\boldsymbol{\alpha}^k$ the thermal expansion coefficients vector, T stands for the over-temperature and:

$$\boldsymbol{\lambda}^k = \mathbf{C}^k \boldsymbol{\alpha}^k \tag{12}$$

According to the used stress and strain ordering, the constitutive equations become:

$$\begin{aligned} \boldsymbol{\sigma}_p &= \mathbf{C}^k_{pp} \boldsymbol{\varepsilon}_{tp} + \mathbf{C}^k_{pn} \boldsymbol{\varepsilon}_{tn} - \boldsymbol{\lambda}^k_p T, \\ \boldsymbol{\sigma}_n &= \mathbf{C}^k_{np} \boldsymbol{\varepsilon}_{tp} + \mathbf{C}^k_{nn} \boldsymbol{\varepsilon}_{tn} - \boldsymbol{\lambda}^k_n T. \end{aligned} \tag{13}$$

Matrices $\mathbf{C}^k_{pp}$, $\mathbf{C}^k_{pn}$, $\mathbf{C}^k_{np}$ and $\mathbf{C}^k_{nn}$ for orthotropic materials are:

$$\begin{gathered} \mathbf{C}^k_{pp} = \begin{bmatrix} C^k_{22} & C^k_{23} & 0 \\ C^k_{23} & C^k_{33} & 0 \\ 0 & 0 & C^k_{44} \end{bmatrix}, \; \mathbf{C}^k_{pn} = \mathbf{C}^{kT}_{np} = \begin{bmatrix} C^k_{12} & C^k_{26} & 0 \\ C^k_{13} & C^k_{36} & 0 \\ 0 & 0 & C^k_{45} \end{bmatrix}, \\ \mathbf{C}^k_{nn} = \begin{bmatrix} C^k_{11} & C^k_{16} & 0 \\ C^k_{16} & C^k_{66} & 0 \\ 0 & 0 & C^k_{55} \end{bmatrix}. \end{gathered} \tag{14}$$

Coefficients C^k_{ij} in Eqs. (14) depend on the engineering material constants and the fibre rotation angle. Their explicit expressions can be found in Reddy [27].

Coefficients $\boldsymbol{\lambda}^k_n$ and $\boldsymbol{\lambda}^k_p$ are:

$$\boldsymbol{\lambda}^{kT}_n = \left\{ \begin{array}{ccc} \lambda^k_1 & \lambda^k_6 & 0 \end{array} \right\}, \quad \boldsymbol{\lambda}^{kT}_p = \left\{ \begin{array}{ccc} \lambda^k_2 & \lambda^k_3 & 0 \end{array} \right\} \tag{15}$$

and they are related to the thermal expansion coefficients $\boldsymbol{\alpha}^k_n$ and $\boldsymbol{\alpha}^k_p$ through the following equations:

$$\begin{aligned} \boldsymbol{\lambda}^k_p &= \mathbf{C}^k_{pp} \boldsymbol{\alpha}^k_p + \mathbf{C}^k_{pn} \boldsymbol{\alpha}^k_n, \\ \boldsymbol{\lambda}_n &= \mathbf{C}^k_{np} \boldsymbol{\alpha}^k_p + \mathbf{C}^k_{nn} \boldsymbol{\alpha}^k_n. \end{aligned} \tag{16}$$

where $\boldsymbol{\alpha}^k_n$ and $\boldsymbol{\alpha}^k_p$ are:

$$\boldsymbol{\alpha}^{kT}_n = \left\{ \begin{array}{ccc} \alpha^k_1 & 0 & 0 \end{array} \right\}, \quad \boldsymbol{\alpha}^{kT}_p = \left\{ \begin{array}{ccc} \alpha^k_2 & \alpha^k_3 & 0 \end{array} \right\}, \tag{17}$$

Stresses are written in terms of the nodal unknowns and the over-temperature by substituting the strain expressions in Eqs. (9) within Eqs. (13):

$$\begin{aligned} \boldsymbol{\sigma}_p &= \mathbf{C}^k_{pp} \mathbf{D}_p F_\tau N_i \mathbf{q}_{\tau \mathbf{i}} + \mathbf{C}^k_{pn} \left(\mathbf{D}_{nx} + \mathbf{D}_{np} \right) F_\tau N_i \mathbf{q}_{\tau \mathbf{i}} - \boldsymbol{\lambda}^k_p T, \\ \boldsymbol{\sigma}_n &= \mathbf{C}^k_{np} \mathbf{D}_p F_\tau N_i \mathbf{q}_{\tau \mathbf{i}} + \mathbf{C}^k_{nn} \left(\mathbf{D}_{nx} + \mathbf{D}_{np} \right) F_\tau N_i \mathbf{q}_{\tau \mathbf{i}} - \boldsymbol{\lambda}^k_n T. \end{aligned} \tag{18}$$

Eqs. (18) are also used to compute the stresses at the nodes in the post-processing.

4 Fourier's Heat Conduction Equation

The over-temperature profile over the beam domain in Eqs. (18) is derived through a Navier-type solution of Fourier's heat conduction equation. For a multi-layered beam, the cross-section Ω is ideally divided into N_{Ω^k} layers along the through-the-thickness direction z:

$$\Omega = \bigcup_{k=1}^{N_{\Omega^k}} \Omega^k, \tag{19}$$

In each layer, the material properties are constant and the Fourier differential equation reads:

$$K_1^k \frac{\partial^2 T^k}{\partial x^2} + K_2^k \frac{\partial^2 T^k}{\partial y^2} + K_3^k \frac{\partial^2 T^k}{\partial z^2} = 0, \tag{20}$$

being K_i^k the thermal conductivity coefficients of the k-th layer. The continuity of temperature and heat flux q_z must be guaranteed at each layer interface, i.e.:

$$\begin{aligned} T_\top^k &= T_\perp^{k+1}, \\ q_{z\top}^k &= q_{z\perp}^{k+1}, \end{aligned} \tag{21}$$

Symbols "$\top$" and "$\perp$" stand for layer's top and bottom, respectively. The heat flux along the through-the-thickness direction is given by:

$$q_z^k = K_3^k \frac{\partial T^k}{\partial z}. \tag{22}$$

In order to obtain a closed form solution, the temperature field is assumed to be independent from the through-the-width coordinate y. Furthermore, the following multiplicative variable separation is assumed:

$$T(x, y, z) = \Theta_n(x)\, \Theta_\Omega(z). \tag{23}$$

Over-temperature boundary conditions on the top and bottom surface of the beam are imposed as:

$$\begin{aligned} T^{N_{\Omega^k}} &= T_\top^{N_{\Omega^k}} \sin(\alpha x), \\ T^1 &= T_\perp^1 \sin(\alpha x), \end{aligned} \tag{24}$$

where $T_\top^{N_{\Omega^k}}$ and $T_\perp^1$ are the maximal amplitudes and α is:

$$\alpha = \frac{m\pi}{l}, \tag{25}$$

with $m \in \mathbf{N}^+$ being the half-wave number along the beam axis. The following temperature field gives a general solution of the considered heat conduction problem:

$$T^k(x, z) = \Theta_n(x)\, \Theta_\Omega^k(z) = \bar{T}^k e^{s^k z} \sin(\alpha x) \tag{26}$$

where $\bar{T}^k$ is an unknown amplitude. The term s is obtained by replacing Eq. (26) into Eq. (20):

$$s_{1,2}^k = \pm \sqrt{\frac{K_1^k}{K_3^k}}\ \alpha. \tag{27}$$

$\Theta_\Omega^k(z)$ in Eq. (26) becomes:

$$\Theta_\Omega^k(z) = \bar{T}_1^k e^{s_1 z} + \bar{T}_2^k e^{s_2 z} \tag{28}$$

or equivalently:

$$\Theta_\Omega^k(z) = C_1^k \cosh\left(\sqrt{\frac{K_1^k}{K_3^k}}\ z\right) + C_2^k \sinh\left(\sqrt{\frac{K_1^k}{K_3^k}}\ z\right). \tag{29}$$

where C_i^k are a set of $2 \cdot N_{\Omega^k}$ unknowns to be obtained form the $2(N_{\Omega^k} - 1)$ boundary conditions in Eqs. (21) and the two conditions at beam top and bottom (Eqs (24)).

5 Element Stiffness Matrix

The governing equilibrium equations of the beam are derived via the Principle of Virtual Displacements (PVD) for a static thermo-elastic analysis:

$$\delta L_{\text{int}} = 0 \tag{30}$$

where L_{int} represents the strain energy and δ stands for a virtual variation. According to the stress and strain vectors splitting, the virtual variation of the strain energy is:

$$\delta L_{\text{int}} = \int_{l_e}\int_{\Omega} \left(\delta \boldsymbol{\epsilon}_{tn}^T \boldsymbol{\sigma}_n + \delta \boldsymbol{\epsilon}_{tp}^T \boldsymbol{\sigma}_p\right) d\Omega dx. \tag{31}$$

where l_e is the element length. When the geometrical relations in Eqs. (9), the constitutive relations in Eqs. (18) and the finite element formulation in Eq. (4) are considered, Eq. (31) reads:

$$\begin{aligned}
\delta L_{\text{int}} = \quad & \delta \mathbf{q}_{\tau i}^T \int_{l_e}\int_{\Omega^k} \Big\{ \left(\mathbf{D}_{nx} N_i\right)^T F_\tau \left[\mathbf{C}_{np}^k \left(\mathbf{D}_p F_s\right) N_j + \mathbf{C}_{nn}^k \left(\mathbf{D}_{np} F_s\right) N_j + \mathbf{C}_{nn}^k F_s \left(\mathbf{D}_{nx} N_j\right)\right] \\
& + \left(\mathbf{D}_{np} F_\tau\right)^T N_i \left[\mathbf{C}_{np}^k \left(\mathbf{D}_p F_s\right) N_j + \mathbf{C}_{nn}^k \left(\mathbf{D}_{np} F_s\right) N_j + \mathbf{C}_{nn}^k F_s \left(\mathbf{D}_{nx} N_j\right)\right] \\
& + \left(\mathbf{D}_p F_\tau\right)^T N_i \left[\mathbf{C}_{pp}^k \left(\mathbf{D}_p F_s\right) N_j + \mathbf{C}_{pn}^k \left(\mathbf{D}_{np} F_s\right) N_j + \mathbf{C}_{pn}^k F_s \left(\mathbf{D}_{nx} N_j\right)\right] \Big\} d\Omega \; dx \; \mathbf{q}_{sj} \\
& - \delta \mathbf{q}_{\tau i}^T \int_{l_e}\int_{\Omega^k} \left[\mathbf{D}_p^T F_\tau N_i \boldsymbol{\lambda}_{\mathbf{p}}^{\mathbf{k}} + \left(\mathbf{D}_{nx}^T + \mathbf{D}_{np}^T\right) F_\tau N_i \boldsymbol{\lambda}_{\mathbf{n}}^{\mathbf{k}}\right] \Theta_\Omega^k \Theta_n \; d\Omega \; dx
\end{aligned}$$

This latter can be written in the following compact vector form:

$$\delta L_{\text{int}} = \delta \mathbf{q}_{\tau i}^T \mathbf{K}_{uu}^{\tau s i j} \mathbf{q}_{sj} - \delta \mathbf{q}_{\tau i}^T \mathbf{K}_{u\theta}^{\tau i}. \tag{32}$$

The components of the stiffness matrix fundamental nucleus $\mathbf{K}_{uu}^{\tau s i j} \in \mathbb{R}^{3\times 3}$ are:

$$\begin{aligned}
K_{uuxx}^{\tau s i j} &= I_{i,xj,x} J_{\tau s}^{11} + I_{i,xj} J_{\tau s,y}^{16} + I_{ij,x} J_{\tau,ys}^{16} + I_{ij} \left(J_{\tau,zs,z}^{55} + J_{\tau,ys,y}^{66}\right) \\
K_{uuxy}^{\tau s i j} &= I_{ij,x} J_{\tau,ys}^{12} + I_{i,xj,x} J_{\tau s}^{16} + I_{ij} \left(J_{\tau,ys,y}^{26} + J_{\tau,zs,z}^{45}\right) + I_{i,xj} J_{\tau s,y}^{66} \\
K_{uuxz}^{\tau s i j} &= I_{ij,x} J_{\tau,zs}^{13} + I_{ij} \left(J_{\tau,zs,y}^{36} + J_{\tau,ys,z}^{45}\right) + I_{i,xj} J_{\tau s,z}^{55} \\
K_{uuyx}^{\tau s i j} &= I_{i,xj} J_{\tau s,y}^{12} + I_{i,xj,x} J_{\tau s}^{16} + I_{ij} \left(J_{\tau,ys,y}^{26} + J_{\tau,zs,z}^{45}\right) + I_{ij,x} J_{\tau,ys}^{66} \\
K_{uuyy}^{\tau s i j} &= I_{ij} \left(J_{\tau,ys,y}^{22} + J_{\tau,zs,z}^{44}\right) + I_{ij,x} J_{\tau,ys}^{26} + I_{i,xj} J_{\tau s,y}^{26} + I_{i,xj,x} J_{\tau s}^{66} \\
K_{uuyz}^{\tau s i j} &= I_{ij} \left(J_{\tau,zs,y}^{23} + J_{\tau,ys,z}^{44}\right) + I_{ij,x} J_{\tau,zs}^{36} + I_{i,xj} J_{\tau s,z}^{45} \\
K_{uuzx}^{\tau s i j} &= I_{i,xj} J_{\tau s,z}^{13} + I_{ij} \left(J_{\tau,ys,z}^{36} + J_{\tau,zs,y}^{45}\right) + I_{ij,x} J_{\tau,zs}^{55} \\
K_{uuzy}^{\tau s i j} &= I_{ij} \left(J_{\tau,ys,z}^{23} + J_{\tau,zs,y}^{44}\right) + I_{i,xj} J_{\tau s,z}^{36} + I_{ij,x} J_{\tau,zs}^{45} \\
K_{uuzz}^{\tau s i j} &= I_{ij} \left(J_{\tau,zs,z}^{33} + J_{\tau,ys,y}^{44}\right) + I_{ij,x} J_{\tau,ys}^{45} + I_{i,xj} J_{\tau s,y}^{45} + I_{i,xj,x} J_{\tau s}^{55}
\end{aligned} \tag{33}$$

$J_{\tau_{(,\phi)} s_{(,\xi)}}^{gh}$ is a cross-section moment and it stands for:

$$J_{\tau_{(,\phi)} s_{(,\xi)}}^{gh} = \int_{\Omega^k} C_{gh}^k F_{\tau_{(,\phi)}} F_{s_{(,\xi)}} \; d\Omega \tag{34}$$

and it is a weighted sum (in the continuum) of each elemental cross-section area where the weight functions account for the spatial distribution of the geometry and the material. $I_{i_{(,x)} j_{(,x)}}$ is an integral over the axial coordinate of the shape functions or their derivatives:

$$I_{i_{(,x)} j_{(,x)}} = \int_{l_e} N_{i_{(,x)}} N_{j_{(,x)}} \; dx \tag{35}$$

These integrals are evaluated numerically through Gauss' quadrature method. In order to correct the shear locking, a selective integration technique is used. Two, three and four quadrature points are used for the full integration for B2, B3 and B4 elements, respectively. One point less is used for selective integration. The selected under-integrated term is I_{ij} in $K^{\tau sij}_{uuxx}$ that is related to shear deformations γ_{xy} and γ_{xz}.
The components of the thermo-mechanical coupling matrix $\mathbf{K}^{\tau i}_{u\theta} \in \mathbb{R}^3$ are:

$$\begin{aligned} K^{\tau i}_{u\theta x} &= I_{\theta_n i_{,x}} J^1_{\theta_\Omega \tau} + I_{\theta_n i} J^6_{\theta_\Omega \tau_{,y}} \\ K^{\tau i}_{u\theta y} &= I_{\theta_n i} J^2_{\theta_\Omega \tau_{,y}} + I_{\theta_n i_{,x}} J^6_{\theta_\Omega \tau} \\ K^{\tau i}_{u\theta z} &= I_{\theta_n i} J^3_{\theta_\Omega \tau_{,z}} \end{aligned} \tag{36}$$

The generic term $J^g_{\theta_\Omega \tau_{(,\phi)}}$ is:

$$J^g_{\theta_\Omega \tau_{(,\phi)}} = \int_{\Omega^k} F_{\tau_{(,\phi)}} \ \lambda^k_g \ \left(\bar{T}^k_1 e^{s_1 z} + \bar{T}^k_2 e^{s_2 z} \right) \ d\Omega. \tag{37}$$

whereas $I_{\theta_n j_{(,x)}}$ stands for:

$$I_{\theta_n i_{(,x)}} = \int_{l_e} N_{i_{(,x)}} \sin(\alpha x) \ dx. \tag{38}$$

where the temperature profile deriving from Fourier exact solution is integrated over the cross-section and along the axis in order to obtain a thermal load variationally consistent with the proposed models Five Gauss' quadrature points are used in order to correctly compute the integral in Eq. (38). Once the approximation order N and the number of nodes per element N^e_n are fixed, the stiffness matrix of the selected element is obtained straightforwardly via summation of the previous nucleus corresponding to each term of the expansion.

6 Numerical Results

The beam support is $[0, l] \times [-a/2, a/2] \times [-b/2, b/2]$ where l is the length, b the thickness and a the width. Slender and very short beams (length-to-side ratio l/b equal to 100 and 3, respectively) are considered. The cross-section is square with $a = b = 1$ m. Simply supported and cantilever beams made of a metallic material or with a laminated orthotropic cross-section are investigated. The boundary conditions for the temperature are: $T_\top = 400$ K and $T_\perp = 300$ K. One half-wave ($m = 1$) is considered, as far as the temperature variation along the beam axis is concerned.
Results are compared with three-dimensional finite element solutions obtained by the commercial software ANSYS. These latter solutions are obtained using the tri-quadratic element "Solid90" for the thermal analysis and the 20-node element "Solid186" for the mechanical problem. Two different meshes (a coarse and a refined one) are considered for three-dimensional finite element analysis. They will be referred to as FEM 3D-C and FEM 3D-R, respectively. About the computational costs, the number of degrees of freedom (DOFs) for the most refined three-dimensional model (a $60 \times 60 \times 60$ mesh) are about $2.7 \cdot 10^6$. Such very refined mesh is required to obtain an accurate description of the stress state induced by the temperature. The DOFs' number (N_{DOFs}) of the present one-dimensional finite elements is function of the expansion order N and the total number of nodes N_n:

$$N_{DOFs} = 3 \cdot \frac{(N+1)(N+2)}{2} \cdot N_n \tag{39}$$

In the case of the most refined model used in the analysis (a 14th-order approximation and 121 nodes) N_{DOFs} is equal to about $4.4 \cdot 10^4$.

6.1 Isotropic beams

Isotropic beams made of an aluminium alloy are first considered. The mechanical properties are: $E = 72$ GPa, $\nu = 0.3$, $K = 121$ W/mK, $\alpha = 23 \cdot 10^{-6}$ K^{-1}.

6.1.1 Simply supported beams

As a first analysis, the convergence of the strain energy versus the number of total nodes is investigated. The results obtained via the finite element method are assessed towards an exact Navier-type solution within the framework of the present formulation, see Carrera and Giunta [15]. Fig. 2 shows the relative strain energy error:

$$\Delta_E = \frac{L_{\text{int}}^{\text{Nav}} - L_{\text{int}}^{\text{FEM}}}{L_{\text{int}}^{\text{Nav}}} \tag{40}$$

versus the dimensionless distance between two consecutive nodes δ_{ii+1}/l for linear, quadratic and cubic elements. The presented results have been obtained for $N = 2$ and $l/b = 10$, nevertheless solution for different expansion orders and length-to-side ratios are very similar. N_n equal to 121 (corresponding to $\delta_{ii+1}/l = 0.008\overline{3}$) is assumed for all the remaining investigations since it ensures a good compromise between accuracy and computational costs. In order to demonstrate that the proposed one-dimensional finite elements are locking-free, the variation of $\hat{u}_z$ defined as:

$$\hat{u}_z = \frac{u_z^{\text{FEM}}}{u_z^{\text{Nav}}} \tag{41}$$

computed at $(x/l, y/a, z/b) = (1/2, 0, 0)$ via B2 elements versus l/b is presented Fig. 3. Selective and full integration strategies are compared and it can be clearly seen that the former is free of locking. Results shows the same strategy is effective in correcting the locking regardless the beam theory order N. As far as tabular results are concerned, the following displacements and stresses:

$$\begin{array}{lll} \tilde{u}_x = u_x\left(0, -\frac{a}{2}, \frac{b}{2}\right) & \tilde{u}_y = u_y\left(\frac{l}{2}, \frac{a}{2}, \frac{b}{2}\right) & \tilde{u}_z = u_z\left(\frac{l}{2}, 0, \frac{b}{2}\right) \\ \tilde{\sigma}_{xx} = \sigma_{xx}\left(\frac{l}{2}, \frac{a}{2}, \frac{b}{2}\right) & \tilde{\sigma}_{xz} = \sigma_{xz}\left(0, -\frac{a}{2}, 0\right) & \tilde{\sigma}_{xy} = \sigma_{xy}\left(0, \frac{a}{4}, \frac{b}{2}\right) \\ \tilde{\sigma}_{zz} = \sigma_{zz}\left(\frac{l}{2}, 0, 0\right) & \tilde{\sigma}_{yy} = \sigma_{yy}\left(\frac{l}{2}, 0, \frac{b}{2}\right) & \tilde{\sigma}_{yz} = \sigma_{yz}\left(\frac{l}{2}, \frac{a}{4}, \frac{b}{4}\right) \end{array} \tag{42}$$

are accounted for. Table 2 shows the displacement components for a slender beam. Convergence of results is obtained for N as low as three and the relative difference with respect to the reference solution is about 0.3%. Results computed via Timoshenko's (TBT) as well as Euler-Bernoulli's (EBT) classical models are also presented to show the importance of higher-order models to study thermal stress problems. They have been obtained using a Navier-type closed form solution that is valid for simply supported beams, see Giunta et al [23]. The displacements for a a very short beam are presented in Table 3. Also in this case results show that lower-order theories yield very accurate predictions: the relative difference for a third-order theory($N_{DOFs} = 3630$) is about 0.4% at worst. The stress components for a very short beam are shown in Tables 4 and 5. Higher-order theories are in very good agreement with the three-dimensional finite element solution. A relative difference smaller than about 1.2% is obtained by N as low as nine. When a 14th-order theory and cubic elements $B4$ are considered, the difference decreases to 0.3% at worst.

6.1.2 Cantilever beams

In the case of isotropic cantilever beams, the following displacements and stresses are considered:

$$\begin{aligned}
&\tilde{u}_x = u_x\left(l, \frac{a}{2}, \frac{b}{2}\right) \qquad \tilde{u}_y = u_y\left(\frac{l}{2}, \frac{a}{2}, \frac{b}{2}\right) \qquad \tilde{u}_z = u_z\left(l, \frac{a}{2}, \frac{b}{2}\right) \\
&\tilde{\sigma}_{xx} = \sigma_{xx}\left(\frac{l}{2}, \frac{a}{2}, \frac{b}{2}\right) \quad \tilde{\sigma}_{xz} = \sigma_{xz}\left(\frac{l}{2}, 0, -\frac{b}{4}\right) \quad \tilde{\sigma}_{xy} = \sigma_{xy}\left(\frac{l}{2}, -\frac{a}{4}, \frac{b}{2}\right) \\
&\tilde{\sigma}_{zz} = \sigma_{zz}\left(\frac{l}{2}, \frac{a}{2}, 0\right) \quad \tilde{\sigma}_{yy} = \sigma_{yy}\left(\frac{l}{2}, 0, \frac{b}{2}\right) \quad \tilde{\sigma}_{yz} = \sigma_{yz}\left(\frac{l}{2}, \frac{a}{4}, \frac{b}{4}\right)
\end{aligned} \tag{43}$$

The displacement components for a slender isotropic beam are presented in Table 6. As for the simply supported case, convergence is observed for $N \geq 3$, relative difference with respect to the three-dimensional analysis being about 1.3% at worst for $\tilde{u}_y$ that is a secondary displacements due to the Poisson's effect. Axial and through-the-thickness displacements are very accurate. Table 7 shows the displacements for a very short beam. Also in this case, a third-order theory yields accurate results (relative difference equal to 0.6%, at worst). Tables 8 and 9 present the stress components. Linear elements $B2$ are not presented for σ_{xy} and σ_{xz} since they have, for these two stress components that are two or three orders of magnitude smaller that the others, a very slow converge. For instance, in the case of a fourth-order model and $N_n = 121$ $\sigma_{xz} = -69.234$ kPa. Increasing N_n, the values converge to the B3 and B4 results. Results obtained by high-order B3 and B4 elements are in very good agreement with the reference solution. For instance, the relative difference is about 1.5% for a ninth-order model, whereas it is about 0.7%, at worst, when N equals 14. Figs. 4 to 6 present the variation of the displacement components over the cross-section in the form of a colour map for a very short beam. The axial location of the cross-section of each component corresponds to the position of its maximum value. A third-order model accurately predicts u_x and u_y, whereas a $N = 8$ theory is considered for u_z whose very small variations are difficult to be well described. As far as the stress components are concerned, results are evaluated at an opportune distance from the clamped end where, as it is well known, stress singularities are present. Stresses are presented in Figs. 7 to 12. A $N = 14$ four-node element has been considered and a very good prediction of the stress field is obtained.

6.2 Laminated beams

A two-layer very short ($l/b = 3$) composite beam with stacking sequence [0/90] is investigated. Lamination sequence starts from the top of the cross-section, laminae are parallel to the Oxy plane and fibres orientation angle is given with respect to the longitudinal direction. The elastic and thermal properties of the material are: $E_L = 172.72$ GPa, $E_T = 6.91$ GPa, $G_{LT} = 3.45$ GPa, $G_{TT} = 1.38$ GPa, $\nu_{LT} = \nu_{TT} = 0.25$, $K_L = 36.42$ W/mK, $K_T = 0.96$ W/mK, $\alpha_L = 0.57 \cdot 10^{-6}\text{K}^{-1}$ and $\alpha_T = 35.60 \cdot 10^{-6}\text{K}^{-1}$. Subscripts "L" and "T" stand for a direction parallel and perpendicular to the fibres, respectively. As in the case of isotropic beam analyses, both simply supported and cantilever boundary conditions are considered.

6.2.1 Simply supported beam

Fig. 13 presents the temperature profile $T(z)$ at the mid-span cross-section for different length-to-thickness ratios. Results provided by three-dimensional FEM match Fourier's heat conduction analytical solution. A non-linear variation along the thickness is observed for $l/b \leq 25$.

As far as displacements and stresses are concerned, they have been evaluated at the following points:

$$\begin{aligned}
&\tilde{u}_x = u_x\left(0, -\frac{a}{2}, -\frac{b}{2}\right) \qquad \tilde{u}_y = u_y\left(\frac{l}{2}, \frac{a}{2}, \frac{b}{2}\right) \qquad \tilde{u}_z = u_z\left(\frac{l}{2}, 0, -\frac{b}{2}\right) \\
&\tilde{\sigma}_{xx} = \sigma_{xx}\left(\frac{l}{2}, 0, \frac{b}{2}\right) \quad \tilde{\sigma}_{xz} = \sigma_{xz}\left(0, -\frac{a}{2}, \frac{b}{4}\right) \quad \tilde{\sigma}_{xy} = \sigma_{xy}\left(0, \frac{a}{4}, \frac{b}{2}\right) \\
&\tilde{\sigma}_{zz} = \sigma_{zz}\left(\frac{l}{2}, 0, \frac{b}{4}\right) \quad \tilde{\sigma}_{yy} = \sigma_{yy}\left(\frac{l}{2}, 0, \frac{b}{2}\right) \quad \tilde{\sigma}_{yz} = \sigma_{yz}\left(\frac{l}{2}, -\frac{a}{4}, \frac{b}{4}\right)
\end{aligned} \tag{44}$$

Table 10 presents the displacement components u_x, u_y and u_z. Results show a very good agreement between advanced one-dimensional models and the three-dimensional solution. For a ninth-order model, the relative difference between beam theories and the reference solution is 0.6%, at worst. The stress components are addressed in Tables 11 and 12. Higher-order theories are accurate: in the case of a 14th-order theory is considered, the relative difference with respect to the three-dimensional solution is 1.7%, at worst.

6.2.2 Cantilever beam

In the case of a cantilever beam, the displacements and stresses shown in Eqs. (45) are considered:

$$\begin{aligned}
&\tilde{u}_x = u_x\left(l, 0, -\frac{b}{2}\right) \qquad \tilde{u}_y = u_y\left(\frac{l}{2}, \frac{a}{2}, \frac{b}{2}\right) \qquad \tilde{u}_z = u_z\left(l, 0, \frac{b}{2}\right) \\
&\tilde{\sigma}_{xx} = \sigma_{xx}\left(\frac{l}{2}, 0, \frac{b}{2}\right) \quad \tilde{\sigma}_{xz} = \sigma_{xz}\left(\frac{l}{2}, -\frac{a}{2}, \frac{b}{4}\right) \quad \tilde{\sigma}_{xy} = \sigma_{xy}\left(\frac{l}{2}, \frac{a}{4}, \frac{b}{2}\right) \\
&\tilde{\sigma}_{zz} = \sigma_{zz}\left(\frac{l}{2}, 0, \frac{b}{4}\right) \quad \tilde{\sigma}_{yy} = \sigma_{yy}\left(\frac{l}{2}, 0, \frac{b}{2}\right) \quad \tilde{\sigma}_{yz} = \sigma_{yz}\left(\frac{l}{2}, -\frac{a}{4}, \frac{b}{4}\right)
\end{aligned} \tag{45}$$

The displacement components are shown in Table 13, whereas Tables 14 and 15 show the stress components. Also in this case, the proposed family of one-dimensional elements yields results very close to the three-dimensional solution. For instance, the displacements via a $N = 9$ B4 element differ by 0.4%, at worst, from the FEM 3D-R solution. The difference is about 1.9% for B3 and B4, at worst, in the case of the stress components. The difference in the B2 solution for $\tilde{\sigma}_{xz}$ and $\tilde{\sigma}_{yz}$ is because results did not converged yet for $N_n = 121$. Cross-section colour maps for displacements and stresses are presented in Figs. 14 to 22. The difference at the interface are due to the fact that some stress components (i.e. σ_{xx} and σ_{yy}) present there high gradients due to the material properties mismatch or that an equivalent single layer approach does not ensure the continuity of the stress components σ_{xz}, σ_{yz} and σ_{zz}. Results are obtained via a $N = 14$, B4 solution. Nevertheless, lower-order theories yield accurate results in the case of displacement: u_x and u_y are well approximated by a third-order theory, while u_z computed by $N = 6$ is coincident to the FEM three-dimensional reference solution. Higher-order models are required for the stresses and a $N = 14$ model yields accurate solutions.

7 Conclusions

A family of one-dimensional finite elements derived through a Unified Formulation has been presented for the thermal stress analysis of three-dimensional isotropic and composite beam structures. The temperature field has been obtained by an exact solution of Fourier heat conduction equation. Slender and very short beams have been investigated for both simply supported and cantilever boundary conditions. Results have been validated through comparison with three-dimensional FEM solutions obtained via the commercial code

ANSYS. Thermo-mechanical problems present a complex three-dimensional stress state that calls for very accurate models especially in the case of laminated configurations with considerable difference in the thermal expansion coefficients. The numerical investigations demonstrated that the proposed family of one-dimensional finite elements allows an accurate yet computationally efficient prediction of the thermoelastic response for all the considered cases.

Acknowledgements

This work has been partially supported by the European Union within the Horizon 2020 research and innovation programme under grant agreement No 642121 and by the Fonds National de la Recherche Luxembourg through the project FNR CORE CO11/MS/1228375 OPTIPIEZO.

References

[1] B.A. Boley and J.H. Weiner. *Theory of thermal stresses*. Dover Publications, 1997.

[2] R. B. Hetnarski and M. R. Eslami. *Thermal stresses - Advanced theory and applications*. Springer, 2009.

[3] L. Gu, Z. Qin, and F. Chu. Analytical analysis of the thermal effect on vibrations of a damped Timoshenko beam. *Mechanical Systems and Signal Processing*, 60:619–643, 2015.

[4] R. N. Pakade, P. N. Khobragade, and N. W. Bagade, S. H. Khobragade. Heat transfer and thermal stresses of semi infinite rectangular beam. *International Journal of Engineering and Innovative Technology*, 4(8), 2015.

[5] T. Sadowski, M. Birsan, and D. Pietras. Multilayered and FGM structural elements under mechanical and thermal loads. Part I: Comparison of finite elements and analytical models. *Archives of Civil and Mechanical Engineering*, 15:1180–1192, 2015.

[6] M. Lezgy-Nazargah. Fully coupled thermo-mechanical analysis of bi-directional FGM beams using NURBS isogeometric finite element approach. *Aerospace Science and Technology*, 45:154–164, 2015.

[7] J. Jeon, A. Muliana, and V. La Saponara. Thermal stress and deformation analyses in fiber reinforced polymer composites undergoing heat conduction and mechanical loading. *Composites Structures*, 111:31–44, 2014.

[8] Y. Xu and D. Zhou. Two-dimensional thermoelastic analysis of beams with variable thickness subjected to thermo-mechanical loads. *Applied Mathematical Modelling*, 36(12):5818–5829, 2012.

[9] A. Carpinteri and M. Paggi. Thermo-elastic mismatch in nonhomogeneous beams. *Journal of Engineering Mathematics*, 61(2-4):371–384, 2008.

[10] P. Vidal and O. Polit. A thermomechanical finite element for the analysis of rectangular laminated beams. *Finite Elements in Analysis and Design*, 42(10):868–883, 2006.

[11] S. Kapuria, P. C. Dumir, and A. Ahmed. An efficient higher order zigzag theory for composite and sandwich beams subjected to thermal loading. *International Journal of Solids and Structures*, 40(24):6613–6631, 2003.

[12] G. L. Ghiringhelli. On the linear three-dimensional behaviour of composite beams. *Composites Part B*, 28(5-6):613 626, 1997.

[13] E. Carrera. Theories and finite elements for multilayered plates and shells: a unified compact formulation with numerical assessment and benchmarking. *Archives of Computational Methods in Engineering*, 10(3):215–296, 2003.

[14] E. Carrera, G. Giunta, and M. Petrolo. *Beam Structures: Classical and Advanced Theories*. Wiley-Blackwell, 2011.

[15] E. Carrera and G. Giunta. Refined beam theories based on a unified formulation. *International Journal of Applied Mechanics*, 2(1):117–143, 2010.

[16] G. Giunta, F. Biscani, S. Belouettar, A. J. M. Ferreira, and E. Carrera. Free vibration analysis of composite beams via refined theories. *Composites Part B: Engineering*, 44(1):540–552, 2013.

[17] G. Giunta, Y. Koutsawa, S. Belouettar, and H. Hu. Static, free vibration and stability analysis of three-dimensional nano-beams by atomistic refined models accounting for surface free energy effect. *International Journal of Solids and Structures*, 50(9):1460–1472, 2013.

[18] G. Giunta, N. Metla, Y. Koutsawa, and S. Belouettar. Free vibration and stability analysis of three-dimensional sandwich beams via hierarchical models. *Composites Part B: Engineering*, 47:326–338, 2013.

[19] A. Catapano, G. Giunta, S. Belouettar, and E. Carrera. Static analysis of laminated beams via a unified formulation. *Composite structures*, 94(1):75–83, 2011.

[20] O. Polit, L. Gallimard, P. Vidal, M. D'Ottavio, G. Giunta, and S. Belouettar. An analysis of composite beams by means of hierarchical finite elements and a variables separation method. *Computers & Structures*, 158:15–29, 2015.

[21] Q.Z. He, H. Hu, S. Belouettar, G. Giunta, K. Yu, Y. Liu, F. Biscani, E. Carrera, and M. Potier-Ferry. Multi-scale modelling of sandwich structures using hierarchical kinematics. *Composite Structures*, 93(9):2375–2383, 2011.

[22] J. Yang, Q. Huang, H. Hu, G. Giunta, S. Belouettar, and M. Potier-Ferry. A new family of finite elements for wrinkling analysis of thin films on compliant substrates. *Composite Structures*, 119:568–577, 2015.

[23] G. Giunta, D. Crisafulli, S. Belouettar, and E. Carrera. A thermo-mechanical analysis of functionally graded beams via hierarchical modelling. *Composite Structures*, 95:676–690, 2013.

[24] G. Giunta, N. Metla, S. Belouettar, A. J. M. Ferreira, and E. Carrera. A thermo-mechanical analysis of isotropic and composite beams via collocation with radial basis functions. *Journal of Thermal Stresses*, 36(11):1169–1199, 2013.

[25] K. J. Bathe. *Finite element procedures.* Prentice hall, 1996.

[26] J. L. Nowinski. *Theory of thermoelasticity with applications.* Sijthoff and Noordhoff, The Netherlands, 1978.

[27] J. N. Reddy. *Mechanics of laminated composite plates and shells. Theory and Analysis.* CRC Press, 2 edition, 2004.

Tables

N	N_u	F_τ
0	1	$F_1 = 1$
1	3	$F_2 = y \quad F_3 = z$
2	6	$F_4 = y^2 \quad F_5 = yz \quad F_6 = z^2$
3	10	$F_7 = y^3 \quad F_8 = y^2 z \quad F_9 = yz^2 \quad F_{10} = z^3$
...	...	...
N	$\frac{(N+1)(N+2)}{2}$	$F_{\frac{(N^2+N+2)}{2}} = y^N \quad F_{\frac{(N^2+N+4)}{2}} = y^{N-1}z \quad \dots \quad F_{\frac{N(N+3)}{2}} = yz^{N-1} \quad F_{\frac{(N+1)(N+2)}{2}} = z^N$

Table 1: Mac Laurin's polynomials terms via Pascal's triangle.

	$-10 \times \tilde{u}_x$		$10^3 \times \tilde{u}_y$			$\tilde{u}_z$	
FEM 3D-R[a]	2.9287		4.6118			2.3347	
FEM 3D-C[b]	2.9287		4.5977			2.3347	
TBT[c]	2.9284		0.0000			2.3303	
EBT[c]	2.9282		0.0000			2.3303	
	B2	B3, B4	B2	B3	B4	B2	B3, B4
$N \geq 3$	2.9286	2.9287	4.6003	4.5997	4.5999	2.3345	2.3347
$N = 2$	2.9286	2.9287	4.6000	4.5994	4.5996	2.3345	2.3347

a: Elements' number $40 \times 40 \times 40$. *b*: Elements' number $20 \times 20 \times 20$.
c: Navier-type solution.

Table 2: Displacement components [m] for a slender isotropic simply supported beam.

	$-10^3 \times \tilde{u}_x$		$10^3 \times \tilde{u}_y$			$10^3 \times \tilde{u}_z$		
FEM 3D-R[a]	9.4694		4.4899			6.1583		
FEM 3D-C[b]	9.4694		4.4899			6.1583		
TBT[c]	8.1330		0.0000			2.0600		
EBT[c]	8.1326		0.0000			2.0600		
	B2	B3, B4	B2	B3	B4	B2	B3	B4
$N = 12$	9.4694	9.4694	4.4903	4.4899	4.4900	6.1585	6.1583	6.1583
$N = 10$	9.4693	9.4693	4.4901	4.4898	4.4898	6.1583	6.1581	6.1582
$N = 8$	9.4697	9.4697	4.4898	4.4895	4.4895	6.1585	6.1584	6.1584
$N = 5$	9.4675	9.4675	4.4810	4.4807	4.4807	6.1584	6.1582	6.1582
$N = 3$	9.4780	9.4780	4.4723	4.4720	4.4720	6.1788	6.1786	6.1786
$N = 2$	9.4306	9.4306	4.2272	4.2269	4.2269	6.0697	6.0695	6.0695

a: Elements' number $40 \times 40 \times 40$. *b*: Elements' number $20 \times 20 \times 20$.
c: Navier-type solution.

Table 3: Displacement components [m] for a very short isotropic simply supported beam.

	$10^{-7} \times \tilde{\sigma}_{xx}$			$10^{-7} \times \tilde{\sigma}_{xy}$			$-10^{-6} \times \tilde{\sigma}_{xz}$		
FEM 3D-R[a]	5.1575			1.4465			9.7330		
FEM 3D-C[b]	5.1647			1.4523			9.7240		
TBT[c]	−4.9189			0.0000			0.0000		
EBT[c]	−4.9215			–[d]			–[d]		
	B2	B3	B4	B2	B3	B4	B2	B3	B4
$N = 14$	5.1661	5.1873	5.1713	1.4425	1.4448	1.4433	9.7450	9.7224	9.7346
$N = 11$	5.1796	5.2018	5.1848	1.4495	1.4518	1.4504	9.7609	9.7382	9.7504
$N = 9$	5.1981	5.2217	5.2033	1.4591	1.4614	1.4600	9.6875	9.6649	9.6770
$N = 7$	5.2329	5.2581	5.2381	1.4786	1.4810	1.4795	9.7292	9.7066	9.7188
$N = 4$	4.3853	4.4123	4.3905	0.9989	1.0013	0.9998	8.5185	8.4960	8.5082
$N = 2$	0.7003	0.7274	0.7056	1.1078	1.1100	1.1086	7.9092	7.8870	7.8990

a: Elements' number $60 \times 60 \times 60$. *b*: Elements' number $20 \times 20 \times 20$.
c: Navier-type solution. *d*: Result not provided by the theory.

Table 4: Stress components $\tilde{\sigma}_{xx}$, $\tilde{\sigma}_{xy}$ and $\tilde{\sigma}_{xz}$ [Pa] for a very short isotropic simply supported beam.

	$-10^{-7} \times \tilde{\sigma}_{yy}$			$10^{-6} \times \tilde{\sigma}_{zz}$			$10^{-6} \times \tilde{\sigma}_{yz}$		
FEM 3D-R[a]		3.0105			7.1816			5.4181	
FEM 3D-C[b]		3.0033			7.2315			5.4812	
	B2	B3	B4	B2	B3	B4	B2	B3	B4
$N = 14$	3.0051	3.0049	3.0103	7.2134	7.2369	7.1733	5.4161	5.4161	5.4161
$N = 11$	3.0103	3.0095	3.0154	7.2201	7.2446	7.1799	5.4032	5.4031	5.4031
$N = 9$	3.0219	3.0204	3.0271	7.2076	7.2306	7.1674	5.4182	5.4182	5.4182
$N = 7$	3.0260	3.0237	3.0312	7.2252	7.2500	7.1851	5.3954	5.3953	5.3953
$N = 4$	2.1536	2.1504	2.1588	6.6861	6.7104	6.6459	2.9825	2.9824	2.9824
$N = 2$	11.108	11.104	11.112	31.938	31.961	31.897	0.2700	0.2700	0.2700

a: Elements' number $60 \times 60 \times 60$. b: Elements' number $20 \times 20 \times 20$.

Table 5: Stress components $\tilde{\sigma}_{yy}$, $\tilde{\sigma}_{zz}$ and $\tilde{\sigma}_{yz}$ [Pa] for a very short isotropic simply supported beam.

	$10 \times \tilde{u}_x$		$10^3 \times \tilde{u}_y$			-$\tilde{u}_z$	
FEM 3D-R[a]	5.8570		4.5429			7.3213	
FEM 3D-C[b]	5.8570		4.6113			7.3211	
	B2	B3, B4	B2	B3	B4	B2	B3,B4
$N \geq 3$	5.8570	5.8569	4.6003	4.5997	4.5999	7.3209	7.3211
$N = 2$	5.8569	5.8569	4.6000	4.5994	4.5996	7.3210	7.3211

a: Elements' number $40 \times 40 \times 40$. *b*: Elements' number $20 \times 20 \times 20$.

Table 6: Displacement components [m] for a slender isotropic cantilever beam.

	$10^2 \times \tilde{u}_x$		$10^3 \times \tilde{u}_y$		$-10^3 \times \tilde{u}_z$		
FEM 3D-R[a]	1.7648		4.4898		6.6082		
FEM 3D-C[b]	1.7649		4.4897		6.6089		
	B2	B3, B4	B2	B3, B4	B2	B3	B4
$N = 12$	1.7650	1.7648	4.4901	4.4898	6.6097	6.6080	6.6079
$N = 10$	1.7650	1.7648	4.4900	4.4896	6.6098	6.6081	6.6080
$N = 8$	1.7651	1.7649	4.4896	4.4893	6.6099	6.6082	6.6082
$N = 5$	1.7652	1.7650	4.4809	4.4805	6.6150	6.6137	6.6137
$N = 3$	1.7667	1.7666	4.4726	4.4722	6.6456	6.6446	6.6446
$N = 2$	1.7651	1.7650	4.2268	4.2265	6.6619	6.6612	6.6611

a: Elements' number $40 \times 40 \times 40$. *b*: Elements' number $20 \times 20 \times 20$.

Table 7: Displacement components [m] for a very short isotropic cantilever beam.

	$10^{-7} \times \tilde{\sigma}_{xx}$			$10^{-4} \times \tilde{\sigma}_{xy}$		$10^{-4} \times \tilde{\sigma}_{xz}$	
FEM 3D-R[a]	5.1972			7.0142		7.9001	
FEM 3D-C[b]	5.2038			7.1993		8.2054	
	B2	B3	B4	B3	B4	B3	B4
$N = 14$	5.2035	5.2269	5.2110	7.0255	6.9671	7.8526	7.8749
$N = 11$	5.2170	5.2414	5.2245	7.1052	6.9644	7.9092	7.8814
$N = 9$	5.2354	5.2612	5.2429	7.1139	6.9644	7.9989	7.8874
$N = 7$	5.2701	5.2975	5.2776	6.7149	6.7495	7.7304	7.8404
$N = 4$	4.4231	4.4525	4.4308	5.7144	5.4920	6.1468	6.0368
$N = 2$	0.6987	0.7248	0.7029	-2.1163	-2.0694	-2.4020	-2.3043

a: Elements' number $60 \times 60 \times 60$. *b*: Elements' number $20 \times 20 \times 20$.

Table 8: Stress components $\tilde{\sigma}_{xx}$, $\tilde{\sigma}_{xy}$ and $\tilde{\sigma}_{xz}$ [Pa] for a very short isotropic cantilever beam.

	$-10^{-7} \times \tilde{\sigma}_{yy}$			$-10^{-7} \times \tilde{\sigma}_{zz}$			$10^{-6} \times \tilde{\sigma}_{yz}$	
FEM 3D-R[a]	3.0045			2.0913			5.3923	
FEM 3D-C[b]	2.9966			2.0830			5.4559	
	B2	B3	B4	B2	B3	B4	B2	B3, B4
$N = 14$	2.9993	2.9990	3.0043	2.0880	2.0868	2.0914	5.3902	5.3902
$N = 11$	3.0044	3.0035	3.0095	2.0917	2.0900	2.0951	5.3774	5.3774
$N = 9$	3.0161	3.0145	3.0211	2.1027	2.1004	2.1061	5.3923	5.3922
$N = 7$	3.0204	3.0179	3.0254	2.1137	2.1107	2.1171	5.3694	5.3694
$N = 4$	2.1505	2.1471	2.1554	1.2802	1.2762	1.2834	2.9727	2.9726
$N = 2$	11.113	11.109	11.118	−7.1294	−7.1326	−7.1253	0.2688	0.2687

a: Elements' number $60 \times 60 \times 60$. *b*: Elements' number $20 \times 20 \times 20$.

Table 9: Stress components $\tilde{\sigma}_{yy}$, $\tilde{\sigma}_{zz}$ and $\tilde{\sigma}_{yz}$ [Pa] for a very short isotropic cantilever beam.

	$-10^3 \times \tilde{u}_x$		$10^3 \times \tilde{u}_y$			$-10^3 \times \tilde{u}_z$	
FEM 3D-R[a]	6.5160		5.3068			8.7798	
FEM 3D-C[b]	6.5161		5.3067			8.7799	
TBT[c]	−0.0471		0.0000			−0.1627	
EBT[c]	−0.0471		0.0000			−0.1627	
	B2	B3, B4	B2	B3	B4	B2	B3,B4
$N = 14$	6.5109	6.5107	5.3072	5.3069	5.3069	8.8172	8.8172
$N = 11$	6.5077	6.5075	5.2930	5.2927	5.2927	8.8294	8.8294
$N = 9$	6.4999	6.4997	5.2944	5.2941	5.2941	8.8341	8.8341
$N = 7$	6.4977	6.4975	5.1728	5.1725	5.1725	8.8606	8.8606
$N = 5$	6.4557	6.4555	5.0304	5.0302	5.0302	8.7907	8.7906
$N = 3$	6.0633	6.0631	4.3927	4.3924	4.3925	8.6835	8.6834
$N = 2$	6.6233	6.6230	1.3257	1.3256	1.3256	8.7811	8.7810

a: Elements' number $40 \times 40 \times 40$. *b*: Elements' number $20 \times 20 \times 20$.
c: Navier-type solution.

Table 10: Displacement components [m] for a very short laminated simply supported beam.

	$-10^{-8} \times \tilde{\sigma}_{xx}$			$10^{-6} \times \tilde{\sigma}_{xy}$			$\text{-}10^{-7} \times \tilde{\sigma}_{xz}$		
FEM 3D-R[a]	1.1519			7.6949			1.6506		
FEM 3D-C[b]	1.1473			7.7425			1.6555		
TBT[c]	0.1708			0.0000			0.0000		
EBT[c]	0.1708			_[d]			_[d]		
	B2	B3	B4	B2	B3	B4	B2	B3	B4
$N = 14$	1.1595	1.1599	1.1597	7.6536	7.6558	7.6540	1.6382	1.6389	1.6385
$N = 11$	1.1558	1.1561	1.1560	7.6922	7.6945	7.6926	1.6433	1.6439	1.6435
$N = 9$	1.1688	1.1691	1.1690	7.7875	7.7897	7.7879	1.7598	1.7605	1.7600
$N = 7$	1.1345	1.1348	1.1347	8.1668	8.1691	8.1672	1.8267	1.8274	1.8269
$N = 4$	1.2616	1.2619	1.2617	6.6134	6.6162	6.6141	1.4939	1.4946	1.4941
$N = 3$	1.0608	1.0610	1.0609	5.2571	5.2596	5.2578	0.8788	0.8794	0.8790
$N = 2$	0.9897	0.9899	0.9899	1.7501	1.7509	1.7503	0.5559	0.5564	0.5561

a: Elements' number $60 \times 60 \times 60$. *b*: Elements' number $20 \times 20 \times 20$.
c: Navier-type solution. *d*: Result not provided by the theory.

Table 11: Stress components $\tilde{\sigma}_{xx}$, $\tilde{\sigma}_{xy}$ and $\tilde{\sigma}_{xz}$ [Pa] for a very short laminated simply supported beam.

	$-10^{-7} \times \tilde{\sigma}_{yy}$			$10^{-6} \times \tilde{\sigma}_{zz}$			$-10^{-6} \times \tilde{\sigma}_{yz}$	
FEM 3D-R[a]	4.0438			5.2706			3.0341	
FEM 3D-C[b]	3.9743			5.2944			3.0583	
	B2	B3	B4	B2	B3	B4	B2	B3, B4
$N = 14$	4.0576	4.0581	4.0581	5.3601	5.3581	5.3581	3.0746	3.0744
$N = 11$	4.0384	4.0390	4.0389	5.4208	5.4188	5.4187	2.8618	2.8616
$N = 9$	4.2086	4.2091	4.2091	4.8464	4.8445	4.8444	3.1198	3.1197
$N = 7$	3.9584	3.9590	3.9589	4.9673	4.9653	4.9653	3.3943	3.3941
$N = 4$	3.0461	3.0467	3.0466	10.190	10.188	10.188	2.0006	2.0004
$N = 3$	4.6004	4.6009	4.6009	19.038	19.036	19.036	1.6835	1.6834
$N = 2$	10.188	10.189	10.189	20.056	20.053	20.053	0.0198	0.0198

a: Elements' number $60 \times 60 \times 60$. b: Elements' number $20 \times 20 \times 20$.

Table 12: Stress components $\tilde{\sigma}_{yy}$, $\tilde{\sigma}_{zz}$ and $\tilde{\sigma}_{yz}$ [Pa] for a very short laminated simply supported beam.

	$10^2 \times \tilde{u}_x$			$10^3 \times \tilde{u}_y$		$10^2 \times \tilde{u}_z$		
FEM 3D-R[a]		1.0544			5.3013		1.2740	
FEM 3D-C[b]		1.0545			5.3012		1.2742	
	B2	B3	B4	B2	B3,B4	B2	B3	B4
$N = 14$	1.0543	1.0542	1.0542	5.3017	5.3014	1.2770	1.2770	1.2770
$N = 11$	1.0540	1.0539	1.0540	5.2874	5.2871	1.2777	1.2777	1.2776
$N = 9$	1.0525	1.0524	1.0524	5.2891	5.2888	1.2789	1.2790	1.2790
$N = 7$	1.0528	1.0527	1.0528	5.1668	5.1665	1.2774	1.2773	1.2773
$N = 4$	1.0424	1.0423	1.0423	5.1206	5.1203	1.2834	1.2835	1.2835
$N = 3$	1.0041	1.0041	1.0041	4.3826	4.3823	1.2085	1.2084	1.2084
$N = 2$	1.0443	1.0443	1.0443	1.3259	1.3259	1.1748	1.1747	1.1747

a: Elements' number $40 \times 40 \times 40$. *b*: Elements' number $20 \times 20 \times 20$.

Table 13: Displacement components [m] for a very short laminated cantilever beam.

	$-10^{-8} \times \tilde{\sigma}_{xx}$			$10^{-5} \times \tilde{\sigma}_{xy}$			$10^{-6} \times \tilde{\sigma}_{xz}$		
FEM 3D-R[a]	1.1976			4.6410			2.3747		
FEM 3D-C[b]	1.1942			4.6604			2.3947		
	B2	B3	B4	B2	B3	B4	B2	B3	B4
$N = 14$	1.2013	1.2038	1.2037	3.5669	4.6279	4.6292	2.6051	2.3536	2.3535
$N = 11$	1.1971	1.1996	1.1994	3.5804	4.6404	4.6417	2.5549	2.3022	2.3022
$N = 9$	1.2104	1.2128	1.2127	3.6198	4.6779	4.6792	2.6416	2.3882	2.3882
$N = 7$	1.1768	1.1792	1.1791	3.4760	4.5540	4.5553	2.7151	2.4626	2.4626
$N = 4$	1.2895	1.2920	1.2918	3.7074	4.9019	4.9029	2.2309	1.9837	1.9836
$N = 3$	1.1263	1.1303	1.1303	2.3786	3.4114	3.4127	0.8488	0.6219	0.6219
$N = 2$	1.0907	1.0946	1.0946	0.1218	0.4345	0.4349	0.9138	0.7354	0.7354

a: Elements' number $60 \times 60 \times 60$. *b*: Elements' number $20 \times 20 \times 20$.

Table 14: Stress components $\tilde{\sigma}_{xx}$, $\tilde{\sigma}_{xy}$ and $\tilde{\sigma}_{xz}$ [Pa] for a very short laminated cantilever beam.

	$-10^{-7} \times \tilde{\sigma}_{yy}$			$10^{-6} \times \tilde{\sigma}_{zz}$			$-10^{-6} \times \tilde{\sigma}_{yz}$	
FEM 3D-R[a]	4.0689			4.8927			3.0258	
FEM 3D-C[b]	3.9995			4.9166			3.0501	
	B2	B3	B4	B2	B3	B4	B2	B3, B4
$N = 14$	4.0824	4.0832	4.0832	4.9833	4.9831	4.9832	3.0698	3.0696
$N = 11$	4.0635	4.0643	4.0643	5.0429	5.0427	5.0427	2.8530	2.8528
$N = 9$	4.2319	4.2327	4.2327	4.4578	4.4577	4.4577	3.1068	3.1067
$N = 7$	3.9861	3.9869	3.9869	4.5607	4.5607	4.5607	3.3787	3.3785
$N = 4$	3.0560	3.0569	3.0569	9.7645	9.7645	9.7646	1.9877	1.9876
$N = 3$	4.6257	4.6267	4.6267	18.790	18.789	18.790	1.6755	1.6754
$N = 2$	10.214	10.214	10.214	19.781	19.781	19.781	0.1973	0.0197

a: Elements' number $60 \times 60 \times 60$. b: Elements' number $20 \times 20 \times 20$.

Table 15: Stress components $\tilde{\sigma}_{yy}$, $\tilde{\sigma}_{zz}$ and $\tilde{\sigma}_{yz}$ [Pa] for a very short laminated cantilever beam.

Figures

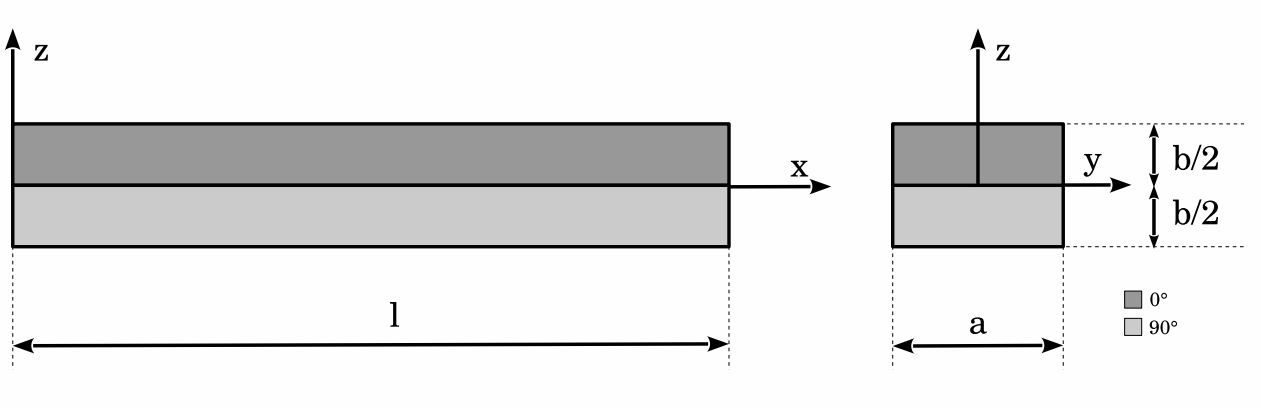

Figure 1: Beam reference system and laminate cross-section.

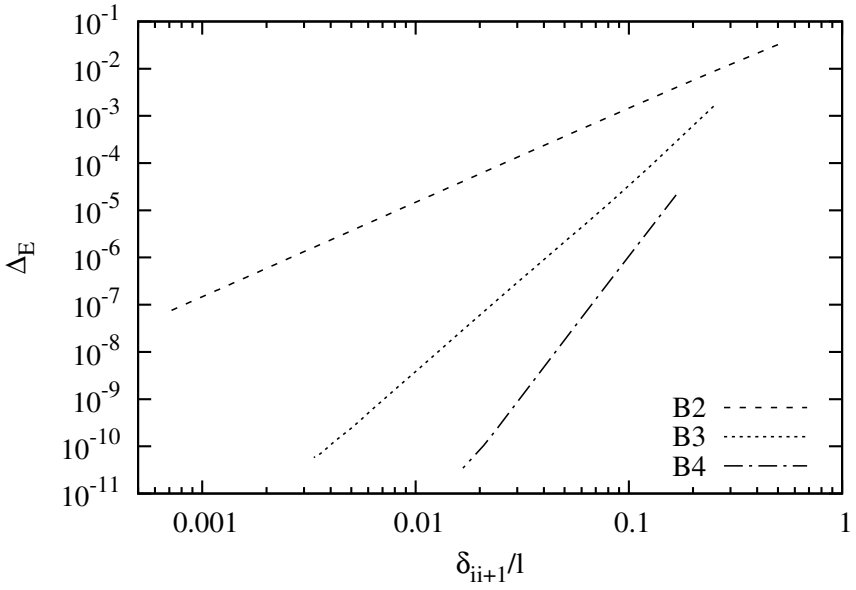

Figure 2: Relative strain energy error (with reference to Navier closed form solution) versus the dimensionless distance between two consecutive nodes, $N = 2$ and $l/b = 10$, simply supported isotropic beam.

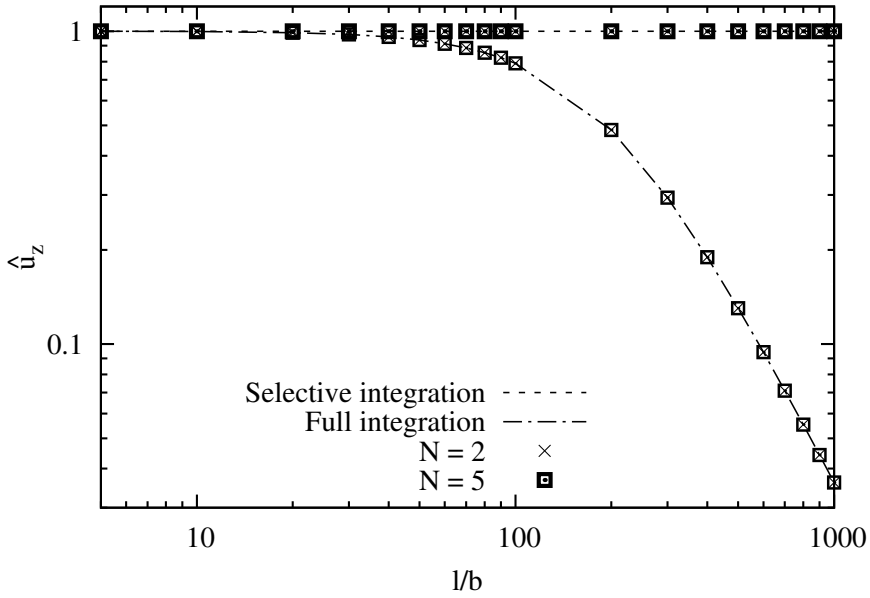

Figure 3: Shear locking correction via selective integration for B2 element, simply supported isotropic beam.

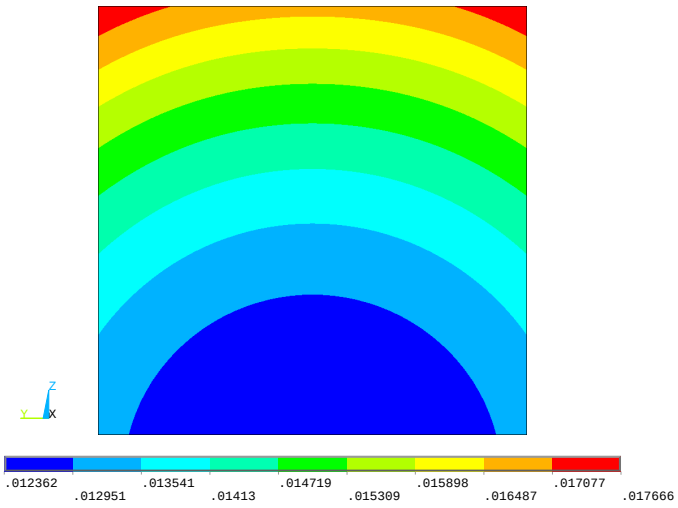

(a)

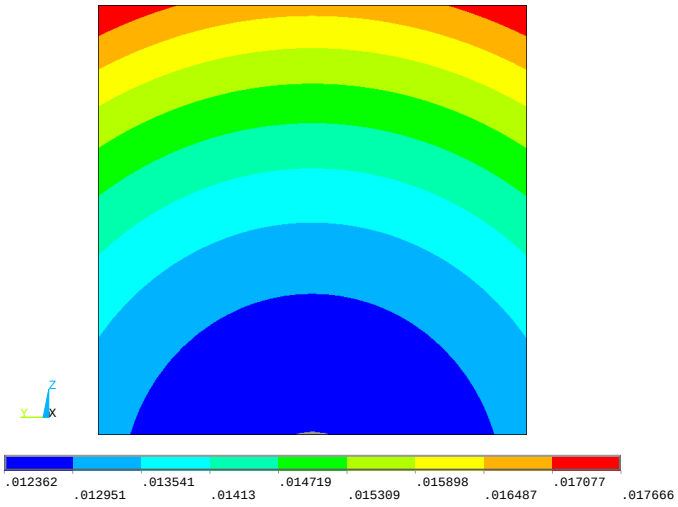

(b)

Figure 4: Axial displacement u_x [m] over the cross-section at $x = l$ via (a) $40 \times 40 \times 40$ FEM 3D-R and (b) $N = 3$, B4 for $l/b = 3$, isotropic cantilever beam.

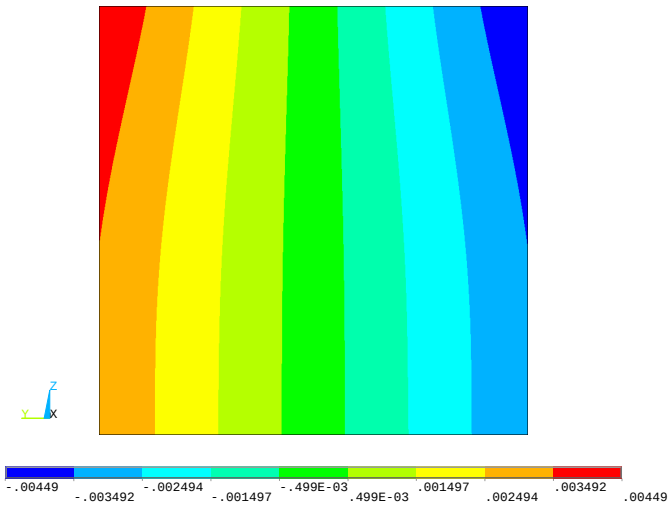

(a)

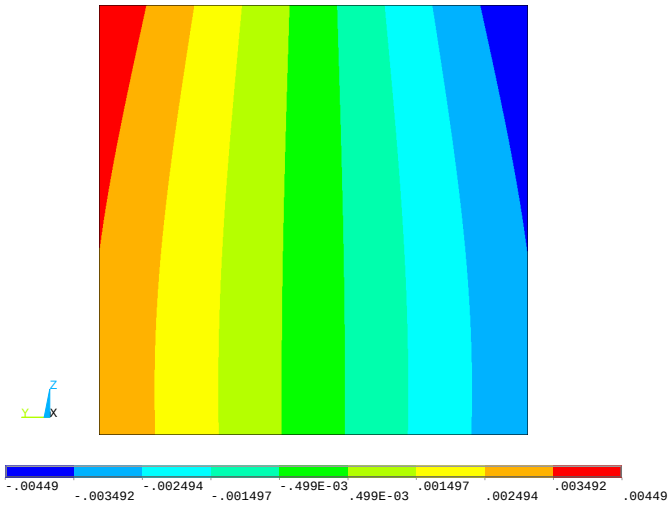

(b)

Figure 5: Through-the-width displacement u_y [m] over the cross-section at $x = l/2$ via (a) $40 \times 40 \times 40$ FEM 3D-R and (b) $N = 3$, B4 for $l/b = 3$, isotropic cantilever beam.

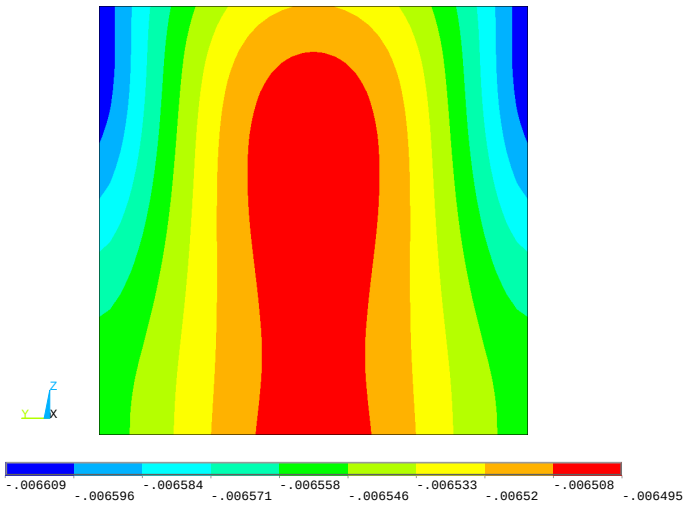

(a)

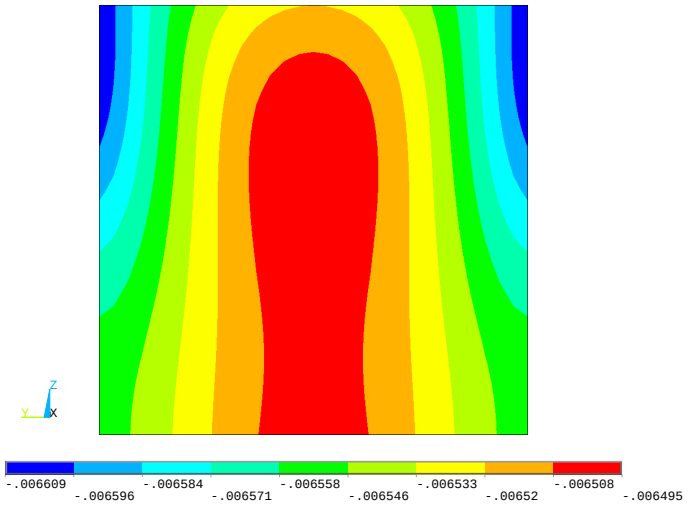

(b)

Figure 6: Through-the-thickness displacement u_z [m] over the cross-section at $x = l/2$ via (a) $40 \times 40 \times 40$ FEM 3D-R and (b) $N = 8$, B4 for $l/b = 3$, isotropic cantilever beam.

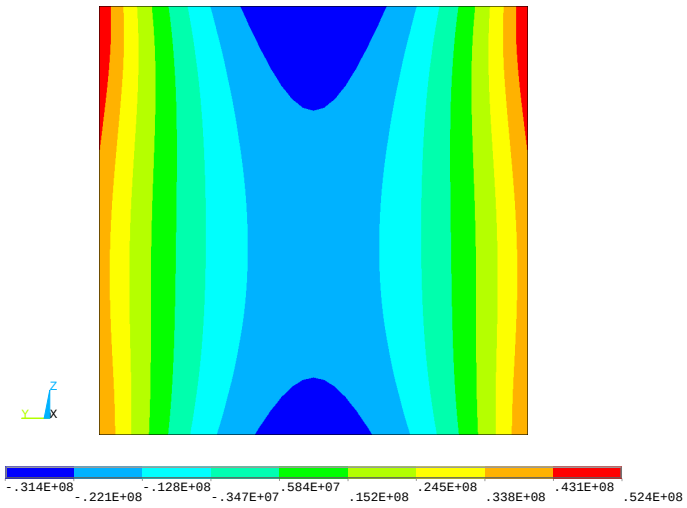

(a)

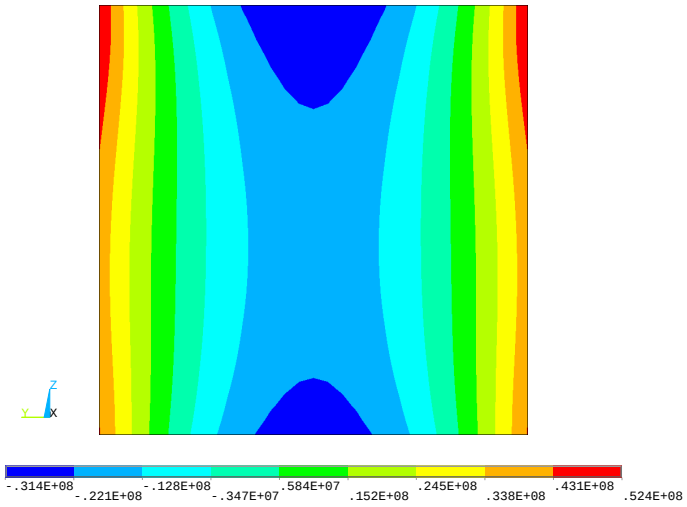

(b)

Figure 7: Axial stress σ_{xx} [Pa] over the cross-section at $x = l/2$ via (a) $40 \times 40 \times 40$ FEM 3D-R and (b) $N = 14$, B4 for $l/b = 3$, isotropic cantilever beam.

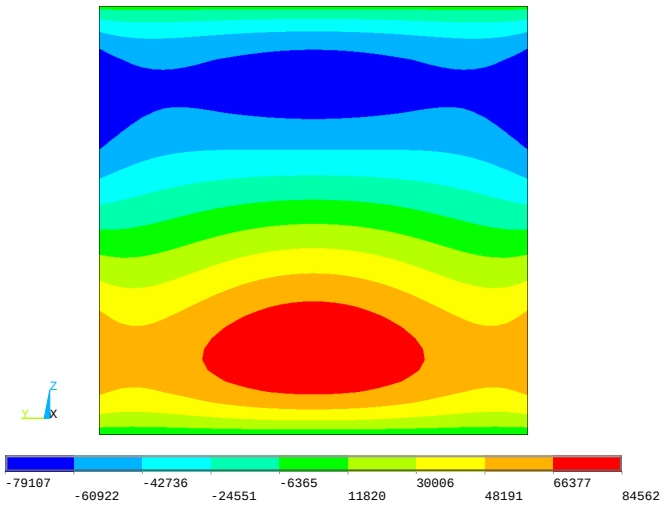

(a)

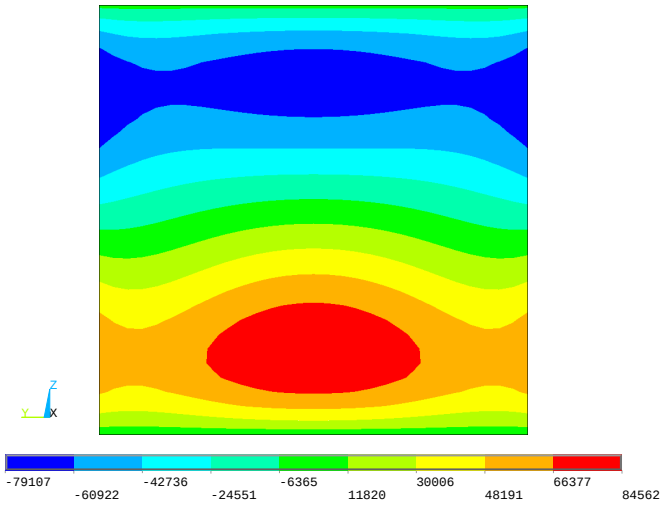

(b)

Figure 8: Shear stress σ_{xz} [Pa] over the cross-section at $x/l = 2$ via (a) $40 \times 40 \times 40$ FEM 3D-R and (b) $N = 14$, B4 for $l/b = 3$, isotropic cantilever beam.

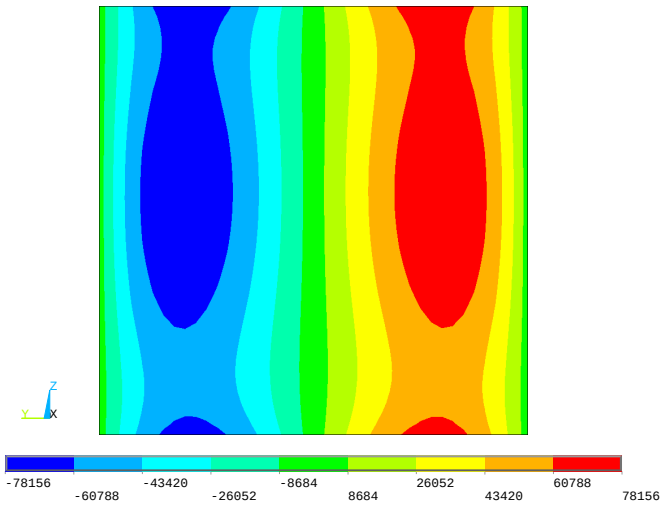

(a)

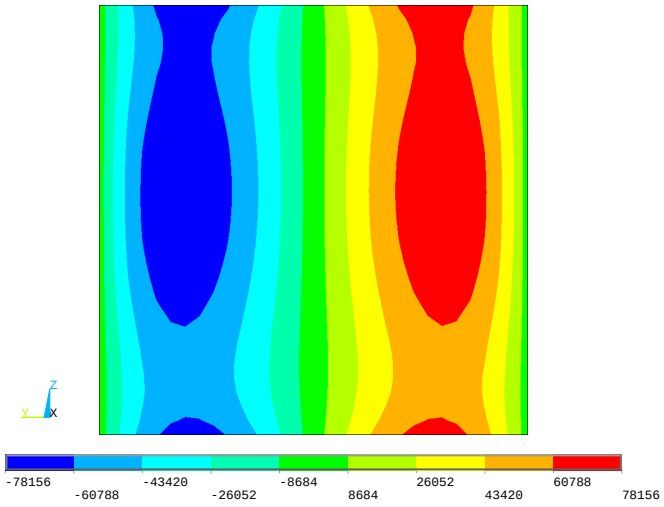

(b)

Figure 9: Shear stress σ_{xy} [Pa] over the cross-section at $x/l = 2$ via (a) $40 \times 40 \times 40$ FEM 3D-R and (b) $N = 14$, B4 for $l/b = 3$, isotropic cantilever beam.

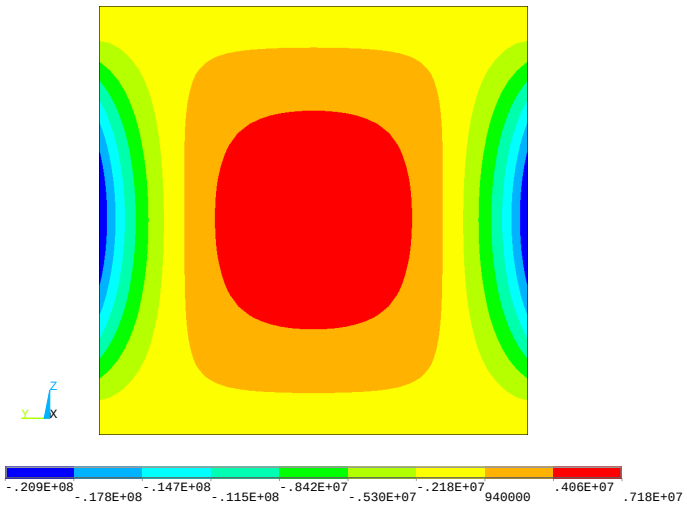

(a)

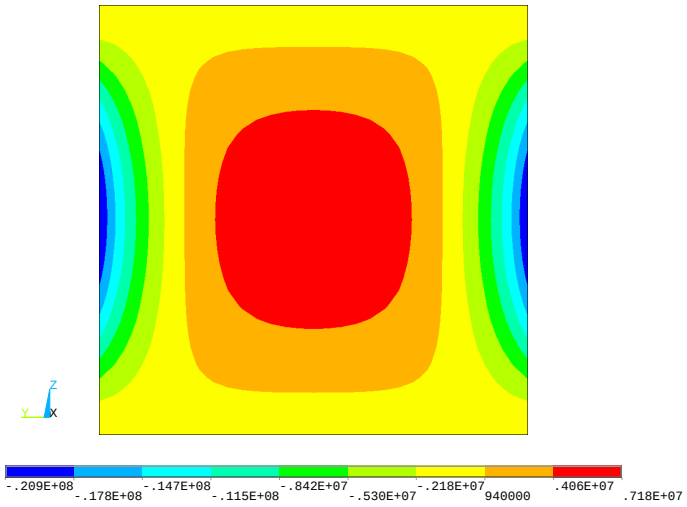

(b)

Figure 10: Through-the-thickness normal stress σ_{zz} [Pa] over the cross-section at $x = l/2$ via (a) $40 \times 40 \times 40$ FEM 3D-R and (b) $N = 14$, B4 for $l/b = 3$, isotropic cantilever beam.

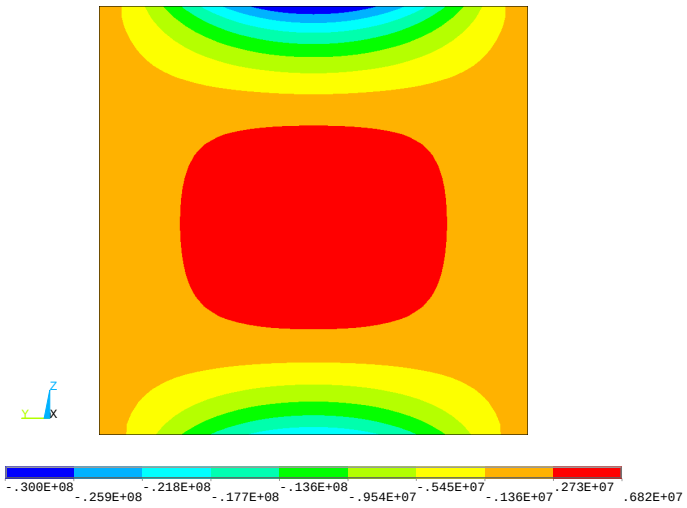

(a)

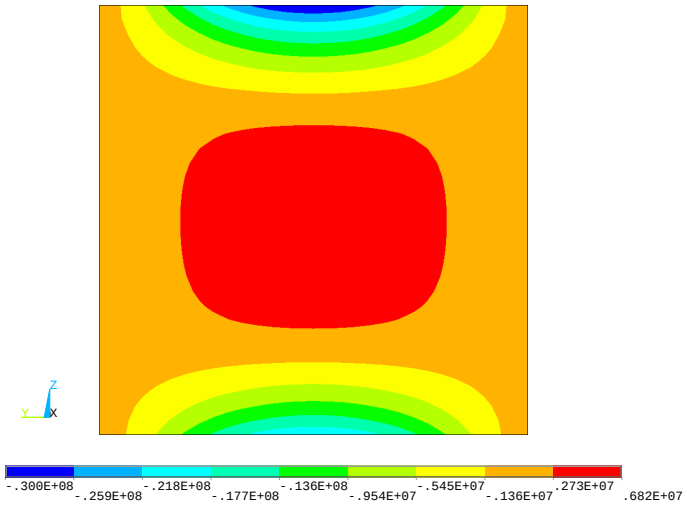

(b)

Figure 11: Through-the-width normal stress σ_{yy} [Pa] over the cross-section at $x = l/2$ via (a) $40 \times 40 \times 40$ FEM 3D-R and (b) $N = 14$, B4 for $l/b = 3$, isotropic cantilever beam.

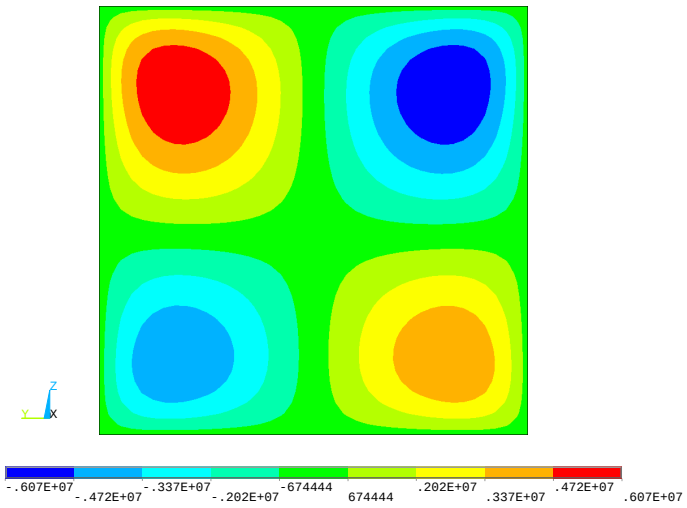

(a)

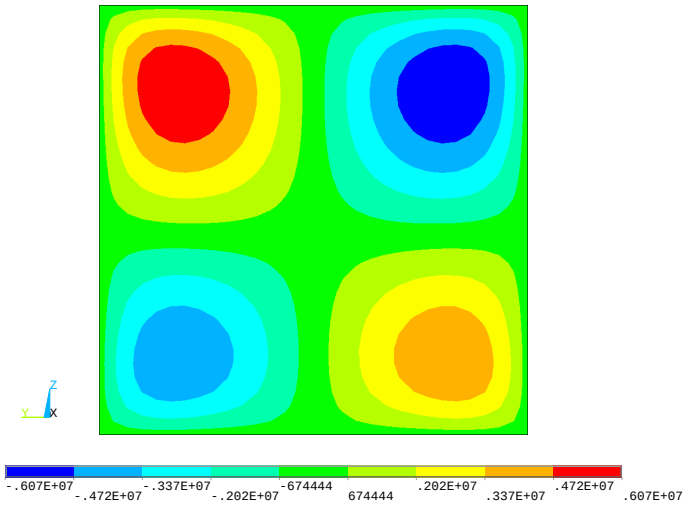

(b)

Figure 12: Shear stress σ_{yz} [Pa] over the cross-section at $x = l/2$ via (a) $40 \times 40 \times 40$ FEM 3D-R and (b) $N = 14$, B4 for $l/b = 3$, isotropic cantilever beam.

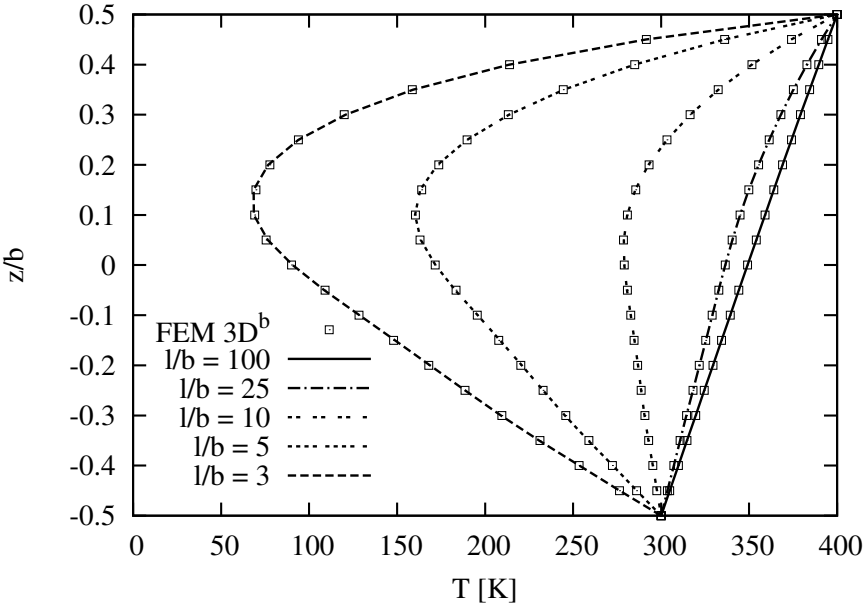

Figure 13: Temperature profile $T(z)$ [K] along the thickness at $x = l/2$ for different length-to-thickness ratios l/b.

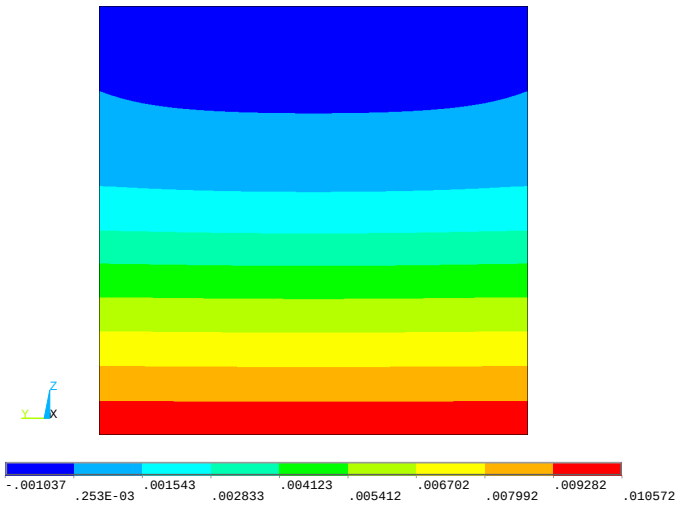

(a)

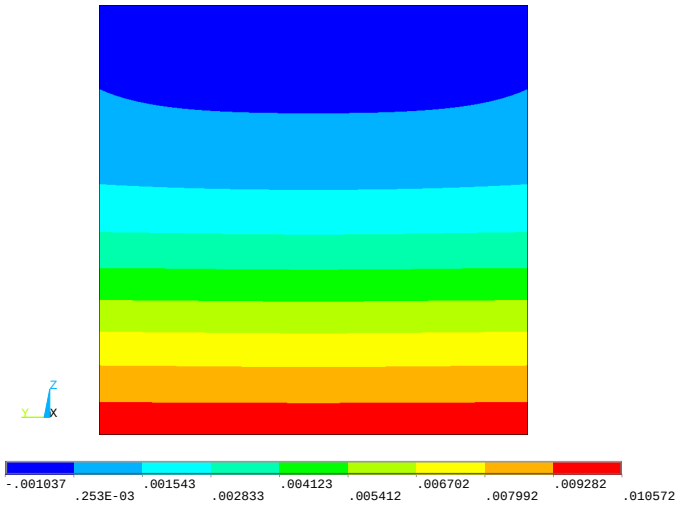

(b)

Figure 14: Axial displacement u_x [m] over the cross-section at $x = l$ via (a) $60 \times 60 \times 60$ FEM 3D-R and (b) $N = 14$, B4 for $l/b = 3$, laminated cantilever beam.

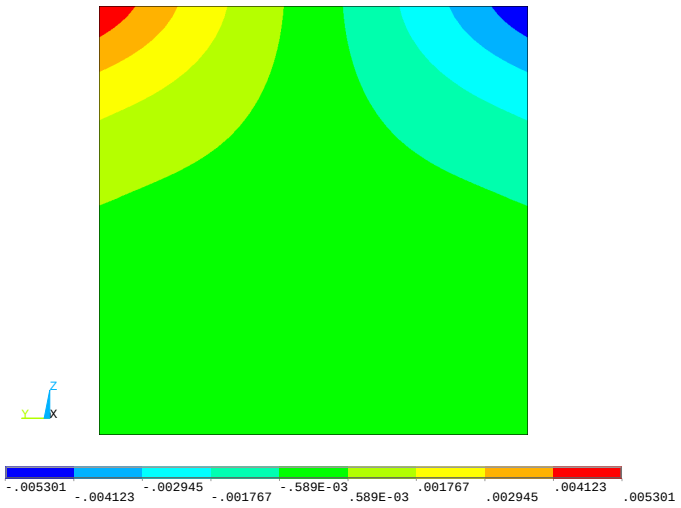

(a)

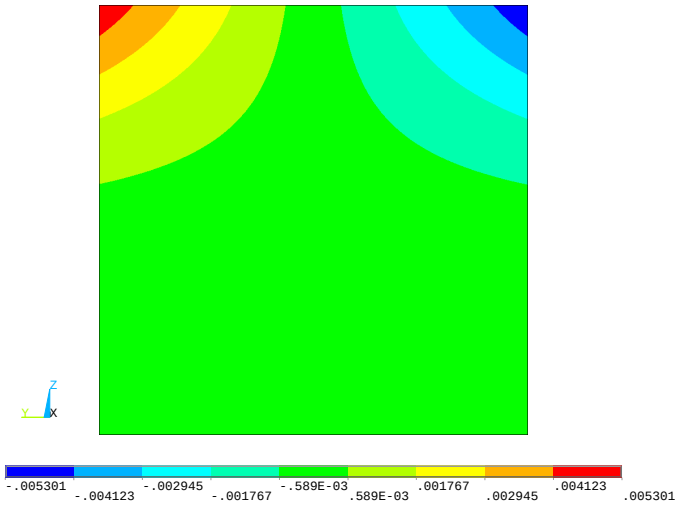

(b)

Figure 15: Through-the-width displacement u_y [m] over the cross-section at $x = l/2$ via (a) $60 \times 60 \times 60$ FEM 3D-R and (b) $N = 14$, B4 for $l/b = 3$, laminated cantilever beam.

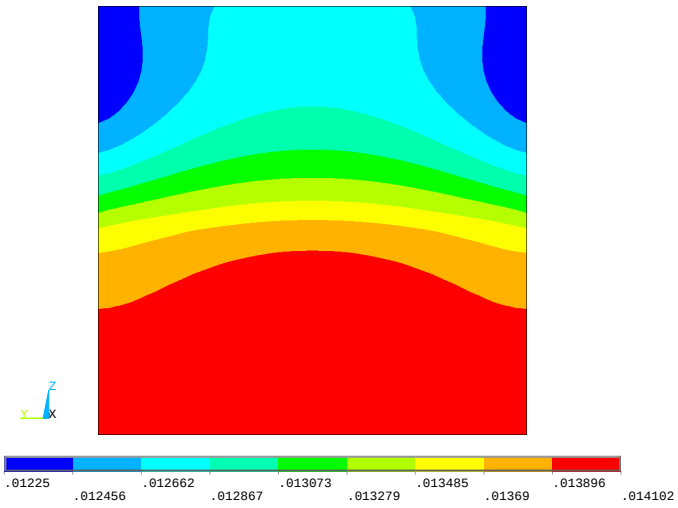

(a)

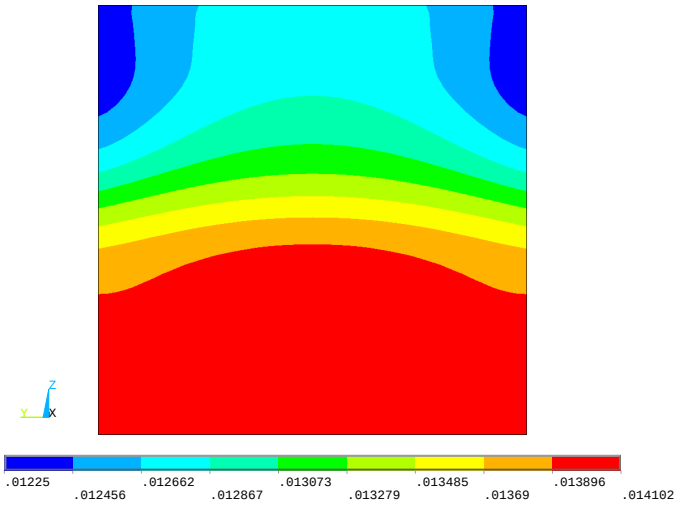

(b)

Figure 16: Through-the-thickness displacement u_z [m] over the cross-section at $x = l/2$ via (a) $60 \times 60 \times 60$ FEM 3D-R and (b) $N = 14$, B4 for $l/b = 3$, laminated cantilever beam.

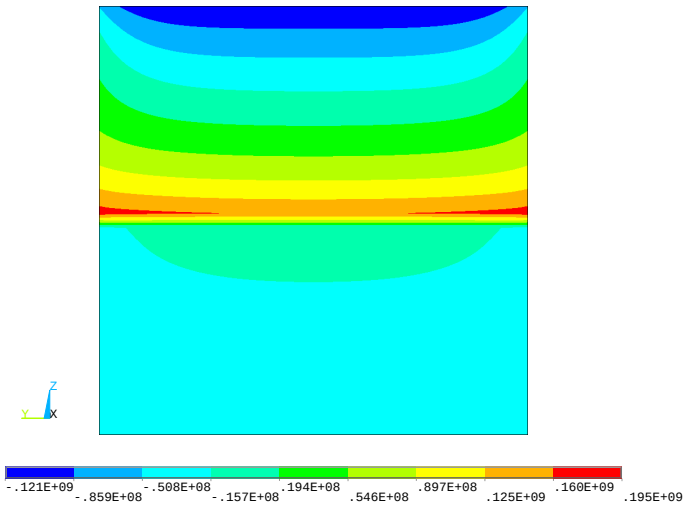

(a)

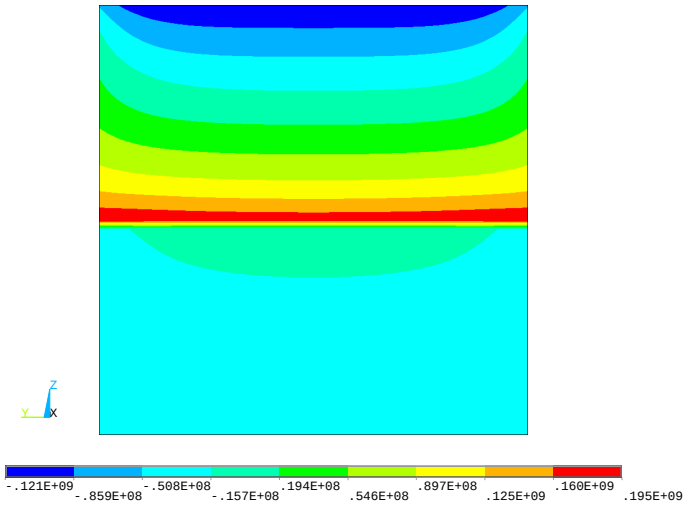

(b)

Figure 17: Axial stress σ_{xx} [Pa] over the cross-section at $x = l/2$ via (a) $60 \times 60 \times 60$ FEM 3D-R and (b) $N = 14$, B4 for $l/b = 3$, laminated cantilever beam.

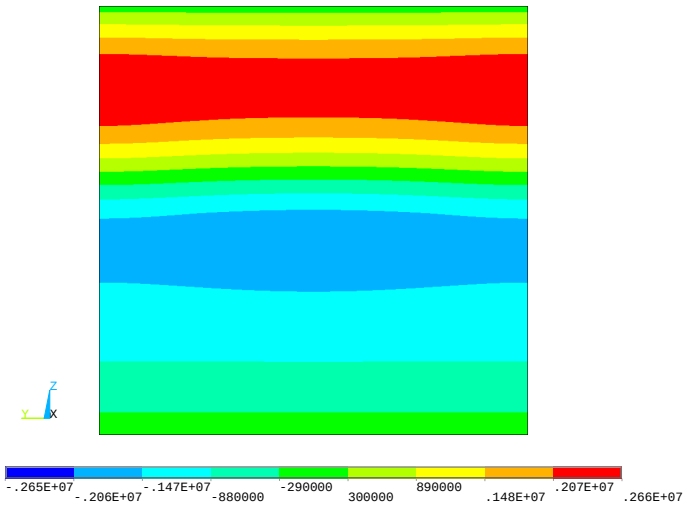

(a)

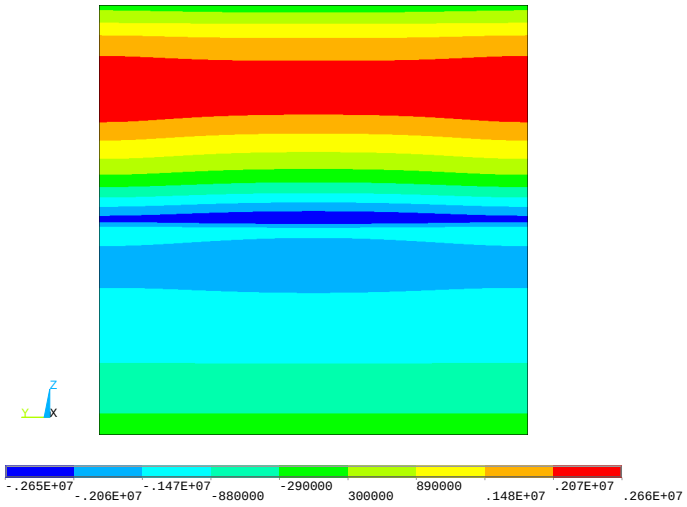

(b)

Figure 18: Shear stress σ_{xz} [Pa] over the cross-section at $x/l = 2$ via (a) $60 \times 60 \times 60$ FEM 3D-R and (b) $N = 14$, B4 for $l/b = 3$, laminated cantilever beam.

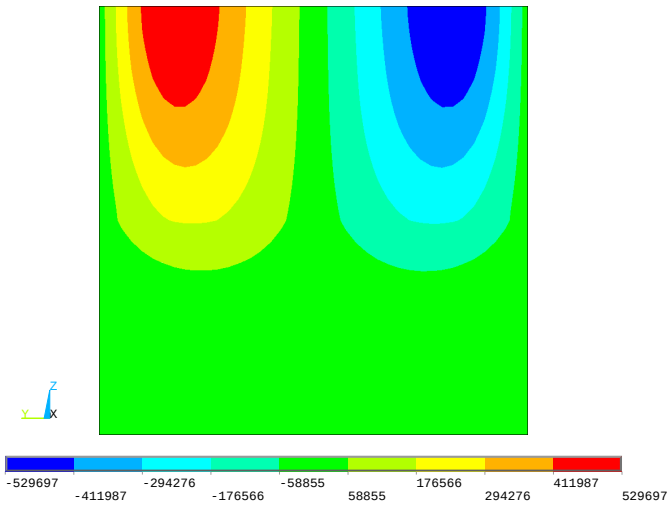

(a)

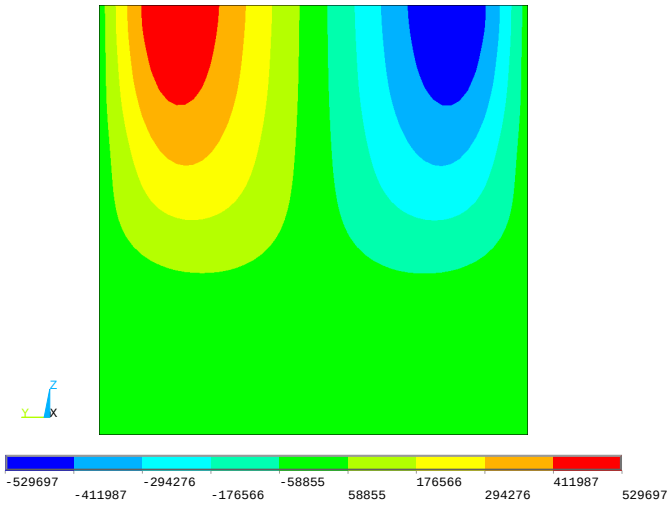

(b)

Figure 19: Shear stress σ_{xy} [Pa] over the cross-section at $x/l = 2$ via (a) $60 \times 60 \times 60$ FEM 3D-R and (b) $N = 14$, B4 for $l/b = 3$, laminated cantilever beam.

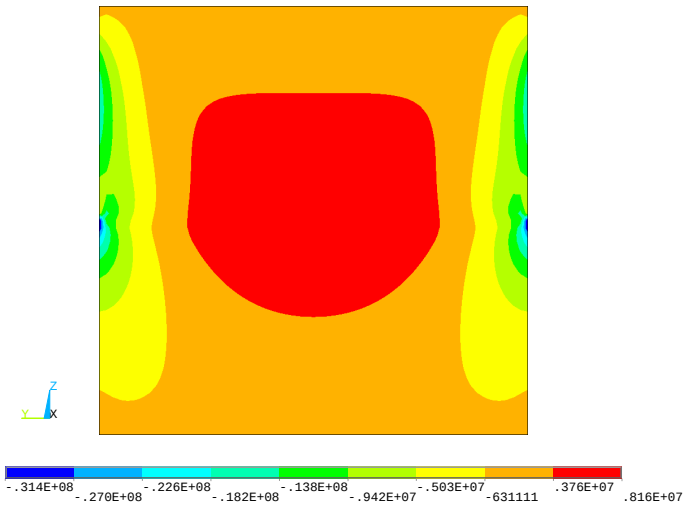

(a)

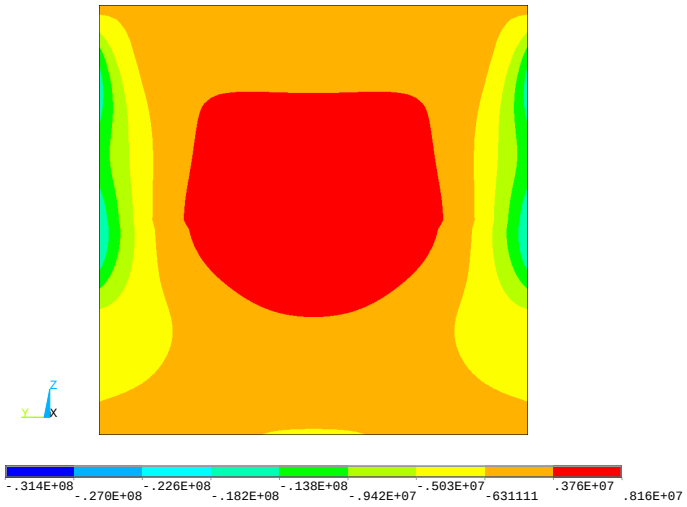

(b)

Figure 20: Through-the-thickness normal stress σ_{zz} [Pa] over the cross-section at $x = l/2$ via (a) $60 \times 60 \times 60$ FEM 3D-R and (b) $N = 14$, B4 for $l/b = 3$, laminated cantilever beam.

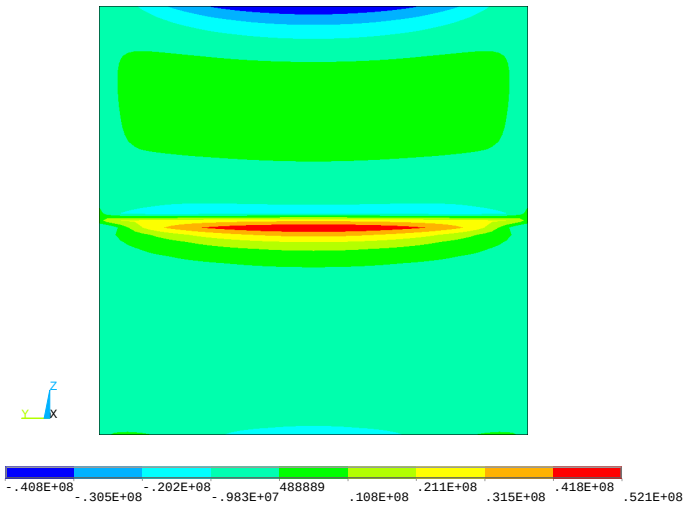

(a)

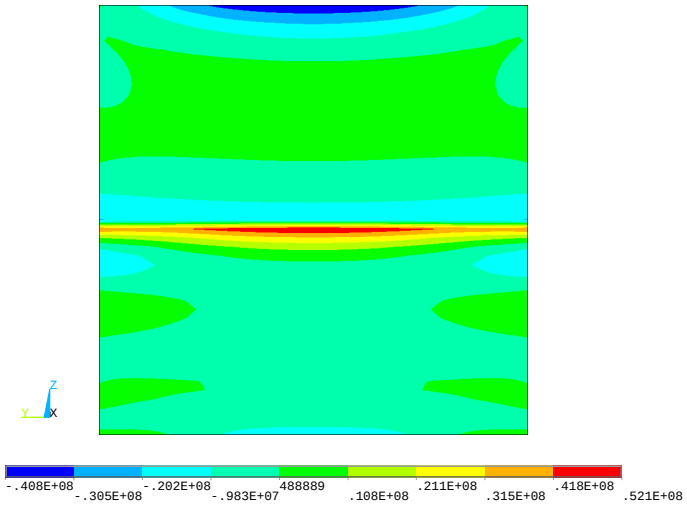

(b)

Figure 21: Through-the-width normal stress σ_{yy} [Pa] over the cross-section at $x = l/2$ via (a) $60 \times 60 \times 60$ FEM 3D-R and (b) $N = 14$, B4 for $l/b = 3$, laminated cantilever beam.

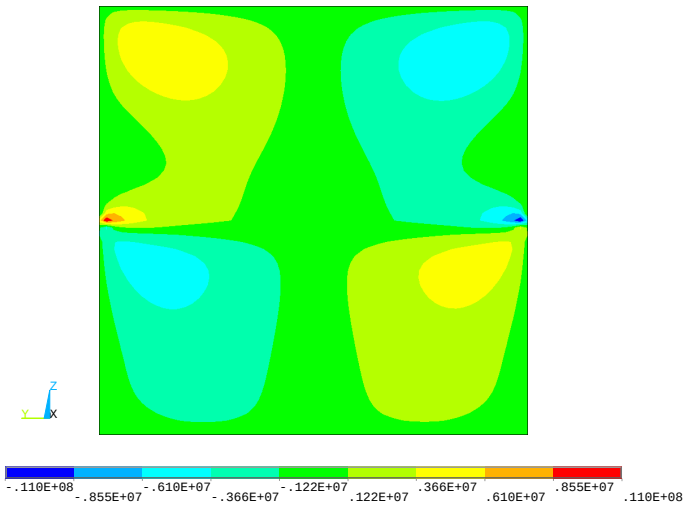

(a)

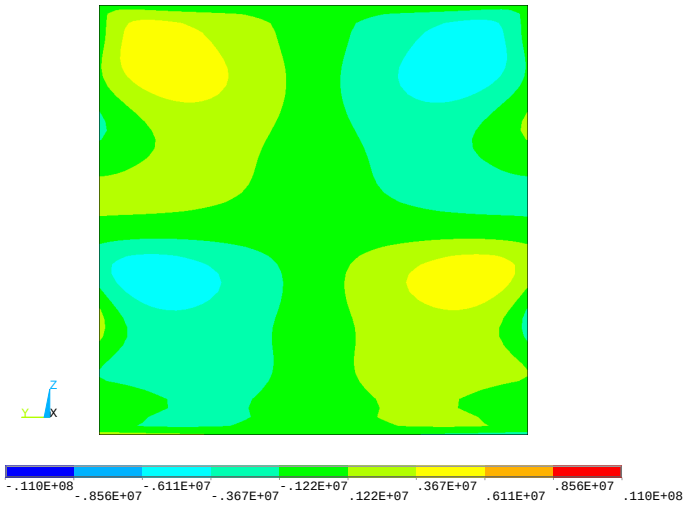

(b)

Figure 22: Shear stress σ_{yz} [Pa] over the cross-section at $x = l/2$ via (a) $60 \times 60 \times 60$ FEM 3D-R and (b) $N = 14$, B4 for $l/b = 3$, laminated cantilever beam.